



OPEN ACCESS

EDITED BY

Xiya Zhang,
China Meteorological Administration, China

REVIEWED BY

Yulong Cui,
Anhui University of Science and
Technology, China
Adolfo Quesada-Román,
University of Costa Rica, Costa Rica
Zhao Zhou,
Xi'an University of Science and
Technology, China

*CORRESPONDENCE

Junxue Ma,
✉ sdnj2mjx@163.com

RECEIVED 09 April 2024

ACCEPTED 29 April 2024

PUBLISHED 13 May 2024

CITATION

Ma J, Chen J and Xu C (2024), Sedimentary records of giant landslide-dam breach events in western Sichuan, China.
Front. Earth Sci. 12:1414763.
doi: 10.3389/feart.2024.1414763

COPYRIGHT

© 2024 Ma, Chen and Xu. This is an open-access article distributed under the terms of the [Creative Commons Attribution License \(CC BY\)](https://creativecommons.org/licenses/by/4.0/). The use, distribution or reproduction in other forums is permitted, provided the original author(s) and the copyright owner(s) are credited and that the original publication in this journal is cited, in accordance with accepted academic practice. No use, distribution or reproduction is permitted which does not comply with these terms.

Sedimentary records of giant landslide-dam breach events in western Sichuan, China

Junxue Ma^{1,2*}, Jian Chen³ and Chong Xu^{1,2}

¹National Institute of Natural Hazards, Ministry of Emergency Management of China, Beijing, China,

²Key Laboratory of Compound and Chained Natural Hazards Dynamics, Ministry of Emergency Management of China, Beijing, China, ³School of Engineering and Technology, China University of Geosciences Beijing, Beijing, China

Introduction: Landslide-dammed lake outburst floods (LLOFs) are common natural disasters in high-mountain regions, posing serious safety threats to residents' livelihoods and properties and causing major damage to engineering facilities. Giant landslides and river damming events commonly occur in the Eastern Tibetan Plateau in southwestern China. Dam failure generate LLOFs that form outburst deposits (ODs). This phenomenon is particularly common in some giant ancient landslide-dammed lakes.

Methods: This study conducted a detailed investigation of the sedimentary characteristics of large-scale landslide-dammed lake outburst deposits in the Dixi Reach of the Upper Minjiang River and Tangjiashan Reach of the Tongkou River Basin, West Sichuan Plateau, China. Meanwhile, typical evidence of high-energy ODs was recorded.

Results and Discussion: The longitudinal distribution of these ODs is similar to an elongated fan-shaped terrace along the river channel, presenting a distinctive sedimentary disordered–sub-ordered–ordered sequence from upstream to downstream. Several typical units of “*sedimentary facies*” are developed in the OD profiles, such as boulder units deposited by high-energy outburst flood (OF) events and the gravel and sand units representing pulsating-flow sedimentary environments during the recession stage. The grain size frequency curves are bimodal, and the granularity accumulated curves are upward convex, which reflect that the detrital characteristics of the sediment source area are mainly composed of coarse gravel and boulders. This indicates that the coarse gravel sediment gradually become decreased from upstream to downstream. Moreover, the OD hydrodynamic intensity displays a gradual weakening, and sediment sorting is improved. From upstream to the downstream, the mean particle-size and sorting of the ODs gradually decrease. The skewness become larger, and the kurtosis of the ODs is distributed in all the types. In addition, the different combinations of quartz sand surface microtextures indicate the transformation from high- to low-energy impacts over a short distance, which is controlled by flood hydrodynamics and regime.

Significance: These sedimentary characteristics of ODs explain the hydrodynamic changes during the propagation of OFs, and are also important records for distinguishing between ODs, and “*normal*” floods.

KEYWORDS

landslide-dammed lake, dam breach, outburst floods (OFs), outburst deposits (ODs), sedimentary characteristics, western Sichuan of China

1 Introduction

Catastrophic flood events are the most destructive natural disasters in the world (O'Connor et al., 2002; Herget and Fontana, 2019; Wang H. et al., 2022), and their complete frequencies and magnitudes cannot be captured by direct observation or measurement (Baker, 2008; Korup and Clague, 2009; Wang et al., 2023a; Benito et al., 2023). It is crucial to reconstruct flood records on the scale of millennia or thousands of years based on geological, geomorphological and chronological flood indicators (Carling, 2013; Chen et al., 2018; Ma et al., 2018; Baker et al., 2022; Baker and Carling, 2022; O'Connor et al., 2022; Quesada-Román et al., 2022). Affected by global warming, the hydrological and climatic changes in the Tibetan Plateau are intensifying, which increases the risk and occurrence of dammed lake OFs (Korup and Montgomery, 2008; Roe et al., 2017; Shugar et al., 2020; Bazai et al., 2021; Taylor et al., 2023). In recent years, an increasing number of studies on catastrophic flood events have been conducted in the Tibetan Plateau (Herget and Fontana, 2019; Baker et al., 2022; O'Connor et al., 2022; Yang et al., 2022). In most of the catastrophic flood cases, dammed lake OFs account for the largest number and widest distribution (Carling, 2013; Srivastava et al., 2017; Liu et al., 2019; Borgohain et al., 2020; Fan et al., 2020; Ma et al., 2022; Yang et al., 2022; Wang et al., 2023b).

There are more than 200 dammed lake OFs known on Earth, with peak discharges exceeding $108 \text{ m}^3/\text{s}$, and their peak discharges are more than 100 times that of the known maximum meteorological flood (O'Connor et al., 2002). In the research by O'Connor et al. (2022), of the 241 cases of dammed lake OFs on Earth with precise peak flow records, 25 were caused by landslide-dammed lake outburst floods (LLOFs). Among these LLOFs, the high mountainous areas of the Tibetan Plateau in southwest China have the highest distribution. These LLOFs often have profound and lasting impacts on regional geomorphological evolution (Korup and Montgomery, 2008; Korup, 2012; Liu et al., 2018; Fan et al., 2020; Ma et al., 2022). Moreover, the outburst floods (OFs) will also cause a large influx of freshwater resources into the ocean, which is closely related to the fluctuations of the Quaternary climate (Teller et al., 2002). Therefore, reconstructing historical floods on the Tibetan Plateau and analyzing their sensitivity to climate conditions will contribute to a better understanding of the impact of future climate change on extreme hydrological events (Knox, 2000; Benito et al., 2015; Støren et al., 2016; Harrison et al., 2018; Baker et al., 2022). In addition, the study of dammed lake OFs has profound significance for river evolution, mountain environmental changes, and human civilization development (Baker, 2008; Peng and Zhang, 2013; Liu et al., 2019; Fan et al., 2020; Wang et al., 2023b; Taylor et al., 2023).

For modern dammed lake OFs, there are usually historical or detailed data records, such as the 1933 Diexi Earthquake (25 August 1933, Ms.7.5), which resulted in 11 landslide-dammed lakes in the Diexi area, Sichuan, China, which breached on October 9 and killed approximately 2,500 people (Li et al., 1986). Another example is the Tangjiashan dammed lake induced by the Wenchuan Earthquake in 2008 (Cui et al., 2012; Peng and Zhang, 2013; Chen et al., 2015; Wang Z. et al., 2022) and the Baige dammed lake in Jinsha River in 2018 (Tian et al., 2020; Zhong et al., 2020; Liu et al., 2021; Zhang et al., 2023), both of which have

detailed data on the OFs. However, there are no records of ancient OF events, particularly those that occurred during the geologic era, which need to be deduced using geomorphology, hydrology, sedimentology, meteorology, and other methods. The OF sediments (outburst deposits, ODs) formed in the lower reaches of the dams are become the most direct evidence of OFs induced by dammed lakes. Analyzing the distribution and sedimentary characteristics of ODs is of great significance for the paleohydrological reconstruction of dammed lake OFs (Dai et al., 2005; Carling, 2013; Chen et al., 2013; Wang P. et al., 2014; Ma et al., 2022; Wang et al., 2023a; Wang et al., 2023b).

Currently, research cases and data on landslide-dammed lakes and LLOFs mainly focus on the causes and processes of landslide damming, lake evolution, dam stability and breach mechanism, hazard assessment and mapping, geomorphic consequences, and sedimentary and controlling effects of the LLOFs on mountain topographic and climatic features (Costa and Schuster, 1988; Huggel et al., 2002; Ermini and Casagli, 2003; Korup et al., 2010; Peng and Zhang, 2012; Walder et al., 2015; van Gorp et al., 2016; Zheng et al., 2021; Wu et al., 2022). Theoretical and model experimental studies have mostly been conducted (Chang and Zhang, 2010; Schmocker et al., 2014; Shi et al., 2015; Jiang et al., 2018; Jiang and Wei, 2019; Zhou et al., 2019; Zhu et al., 2019; Zhong et al., 2021). However, there are still some unresolved problems in the study of the relationship between the sedimentation process of ODs and the dynamic characteristics of flood evolution. The theoretical system is not yet perfect, and there are conflicts among many pieces of evidence. Therefore, new sedimentary evidence is needed to support these issues (Lord and Kehew, 1987; Cutler et al., 2002; Borgohain et al., 2020; Wang et al., 2023a). An abundance of ODs was discovered to be preserved in the Diexi Reach of the Upper Minjiang River and Tangjiashan Reach of the Tongkou River Basin (Ma et al., 2018; Jiang and Wei, 2020; Jiang et al., 2021; Ma et al., 2022). These ODs were formed by LLOFs induced by a giant ancient landslide-dammed lake and the Tangjiashan dammed lake, respectively, and they have good comparability in terms of deposition distribution, sedimentary characteristics and profile structures. From ancient to modern times, these two cases present distinct contrasts and distinctive features, providing important sedimentary evidence for the giant landslide-dam breach events in Western Sichuan, China. The main purposes of this study are as follows: i) to explore the geomorphological and sedimentary characteristics of the ODs in the Diexi Reach of the Upper Minjiang River and Tangjiashan Reach of the Tongkou River Basin; ii) to analyze the hydraulic characteristics of the LLOFs; and iii) to explore the discrimination indicators between dammed lake OF events and other "normal flood" events. This study has a good practical significance for flood disaster prediction and mitigation of dammed-lakes' failures at present and in the future at the southeastern margin of the Tibetan Plateau.

2 Regional settings

The West Sichuan Plateau acts as a transition zone between the Tibetan Plateau (the First Gradient Terrain, and the altitude is more than 3,500 m) and the Sichuan Basin (the Second Gradient Terrain, and the altitude is between 1,000 and 2,000 m)

(Figure 1A), with a vertical drop of more than 2,000 m between the two terrains. This region is in the “*Tethys–Himalayas–Tectonic Zone*,” surrounded by triangular geological structures composed of the Songpan–Ganzi geosynclinal fold belt (NWW direction), the West Qinling geosynclinal fold belt (EW direction), and the Longmenshan–Minshan fault zone (NE direction). Some complex tectonic structures have developed in this area, such as the well-known “*NS-Trending Tectonic Zone*” (Wang et al., 2011; Zhang, 2013) and several groups of major active fault zones—the Longmenshan–Minshan, Minjiang, Huya, and Yingxiu–Beichuan fault zones (Figure 1A). The study area is characterized by frequent fault activities, frequent earthquakes and poor stability. Several historical large-magnitude earthquakes have occurred in the past 2,000 years, including some large-scale ancient seismic activities (Ran et al., 2008; Wang et al., 2011).

The Diexi Reach belongs to the middle section of the Upper Minjiang River, located between Songpan County (upstream) and Maoxian County (downstream) in A’ba Prefecture, Sichuan Province, with distances of 80 km and 60 km, respectively (Figure 1A). Deep incisions along the Upper Minjiang River resulted from intense tectonic uplift at the West Sichuan Plateau in the southeastern margin of the Tibetan Plateau since the late Cenozoic (Li et al., 1986; Burchfiel et al., 1995; Xue et al., 1998; Gao et al., 2002). This region is characterized by high mountains and deep valleys with heights of ~3,000 and 1,500 m, respectively. Owing to the deep incisions, U- or V-shaped gorges are the main features of the valleys, with steep slopes, mostly above 60°. The valleys are relatively wide, ranging from tens of meters to several hundred meters. Many small canyons are distributed on both sides of the river, mostly alternating between mountains and rivers. According to the regional geological survey report of the Sichuan Province (RGSTS, 1975), the lithology in the area mainly consists of sandstone, phyllite, limestone, and gneiss. It is evident that these rocks have experienced different degrees of regional metamorphism (Figure 1B). The drought phenomenon in this region is relatively serious, belonging to the subtropical plateau–continent monsoon climate, with an average annual rainfall of only 420 mm. The Minjiang River is a perennial hydrographic system in this region, with an annual average flow of 21.178 billion m³, which is mainly supplied by atmospheric precipitation (Ma et al., 2022). In addition, the Diexi Haizi dammed lakes, caused by the 1933 Diexi Earthquake are composed of Shanghaizi (or Dahaizi) Lake and Xiahaizi (or Xiaohaizi) Lake, with a maximum width of 692 m, ~80 m in depth and length of more than 10 km (Figure 1C). The total catchment area on the Diexi Haizi is approximately 3.15 km², among which, the catchment areas of the Shanghaizi and Xiahaizi Lakes are 1.8 and 1.35 km², respectively, and the corresponding volumes are 7×10^7 and 5×10^7 m³, respectively (Figure 1C).

The Tangjiashan dammed lake is located in the Tongkou Reach of the Fujiang River. The landslide dam is approximately 6.5 km away from Beichuan County downstream and approximately 74.5 km from the Diexi dammed lake. The Tangjiashan Reach is a V-shaped valley with a steep right bank (40°–60°) and a gentle left bank (~30°) terrain, and many small gullies are developed. The water level in the Tangjiashan Reach is approximately 0.5–4.0 m, with a water surface elevation of approximately 664.7 m (dry season) and width of <300 m before the 2008 Wenchuan Earthquake occurred (Cui et al., 2012; Chen et al., 2015). The Tangjiashan region has

a subtropical monsoon climate with an uneven distribution of rainfall and an average annual rainfall of 1,335 mm, which is concentrated in summer (May to September). The inflow during the formation stage of the barrier lake is approximately 80 m³/s (Bo et al., 2015; Wang Z. et al., 2022). The landslide dam in the Tangjiashan Reach is a long strip with a length of 803.4 m along the river and a maximum width of 611.8 m in the transverse direction. The top width of the landslide dam is approximately 300–310 m, and the lowest and highest points of the dam crest have elevations of 752.1 m and 793.9 m, respectively. The estimated volume is approximately 20.37 million m³, and the catchment area of the Tangjiashan dammed lake is 3,550 km². On 21 May 2008, the lake water elevation reached 711.0 m, with a volume of approximately 72.5 million m³. A relatively wide new river channel was formed after the completion of discharge, with a curved shape protruding toward the right bank. The length and bottom width of the new central river channel are approximately 890 m and 100 m, respectively, with a depth of 40–60 m (Cui et al., 2012; Chen et al., 2015; Zhao et al., 2018; Xiong et al., 2022).

3 Materials and methods

3.1 Sedimentological investigation

Previous studies have commonly used slack water deposits (SWDs) (Jarrett and England, 2002) as paleo-stage indicators (PSIs) of ancient floods (Guo et al., 2017; Ruiz-Bellet et al., 2017). Paleoflood SWD-PSI is a type of suspended sediment with a sharp decrease in flow velocity under high water level stagnation (or backwater) environments, usually consisting of fine-grained sand, clay and silt with parallel bedding (Guo et al., 2023; Mao et al., 2023). It is considered to be a complete paleoflood deposit with significant precise water level indicators (Baker and Carling, 2022; Benito et al., 2022). SWDs are widely used for reconstructing smaller-scale paleoflood events (Benito et al., 2003; Baker, 2008; Huang et al., 2010; Wang L. et al., 2014; Mao et al., 2016). However, SWDs in the alpine canyon river system in a large-magnitude and high-energy OF environment are difficult to preserve but instead form ODs mainly composed of coarse gravel (Carling, 2013). The OF induced by a giant landslide-dammed lake is a typical “*Mega-flood*” (Baker and Carling, 2022; O’Connor et al., 2022), which forms an abundance of ODs on the bank and riverbed downstream of the dam (Wang P. et al., 2014; Chen et al., 2018; Ma et al., 2018).

Typical large-scale landslide-dammed lake ODs were discovered in the Diexi Valley of the Upper Minjiang River and the Tangjiashan Valley of the Tongkou River. The sedimentary characteristics of these ODs are significantly different from those of mountain river facies, normal floods, alluvial fan, and debris flow. In this study, we focused on examining and analyzing the geomorphologic environment and sedimentary sequences of the ODs in the Diexi Valley of the Upper Minjiang River and the Tangjiashan Valley of the Tongkou River, including the following: i) investigating the outcropping sequence strata and geomorphic characteristics of ODs, such as exposed sites, channel expansions and constraints, channel bends, channel branching, and obstacle shadows; ii) recording the sedimentary characteristics of profile outcrops, including bed geometry, bed thickness, bed contacts, color, grain size, texture, and internal

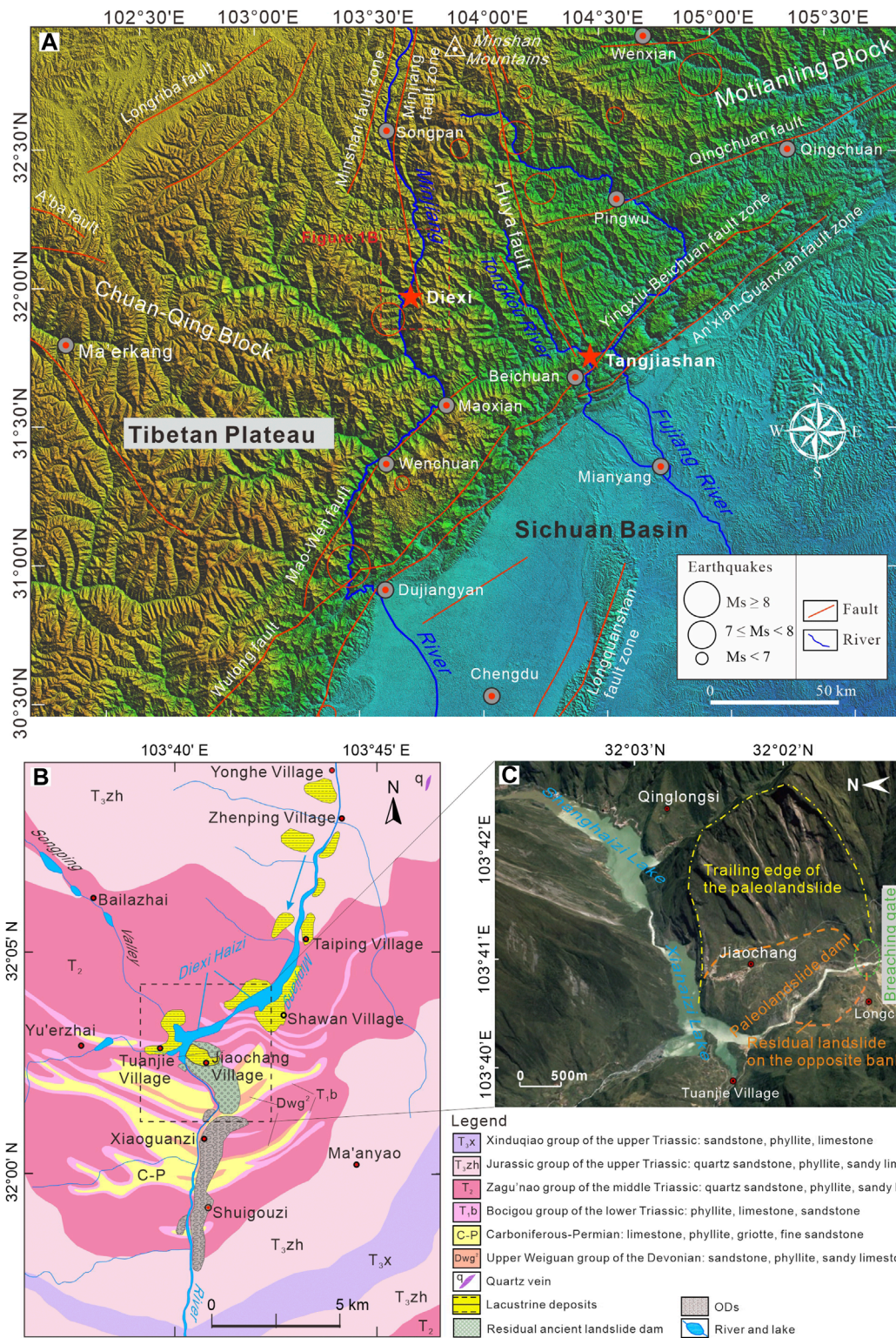
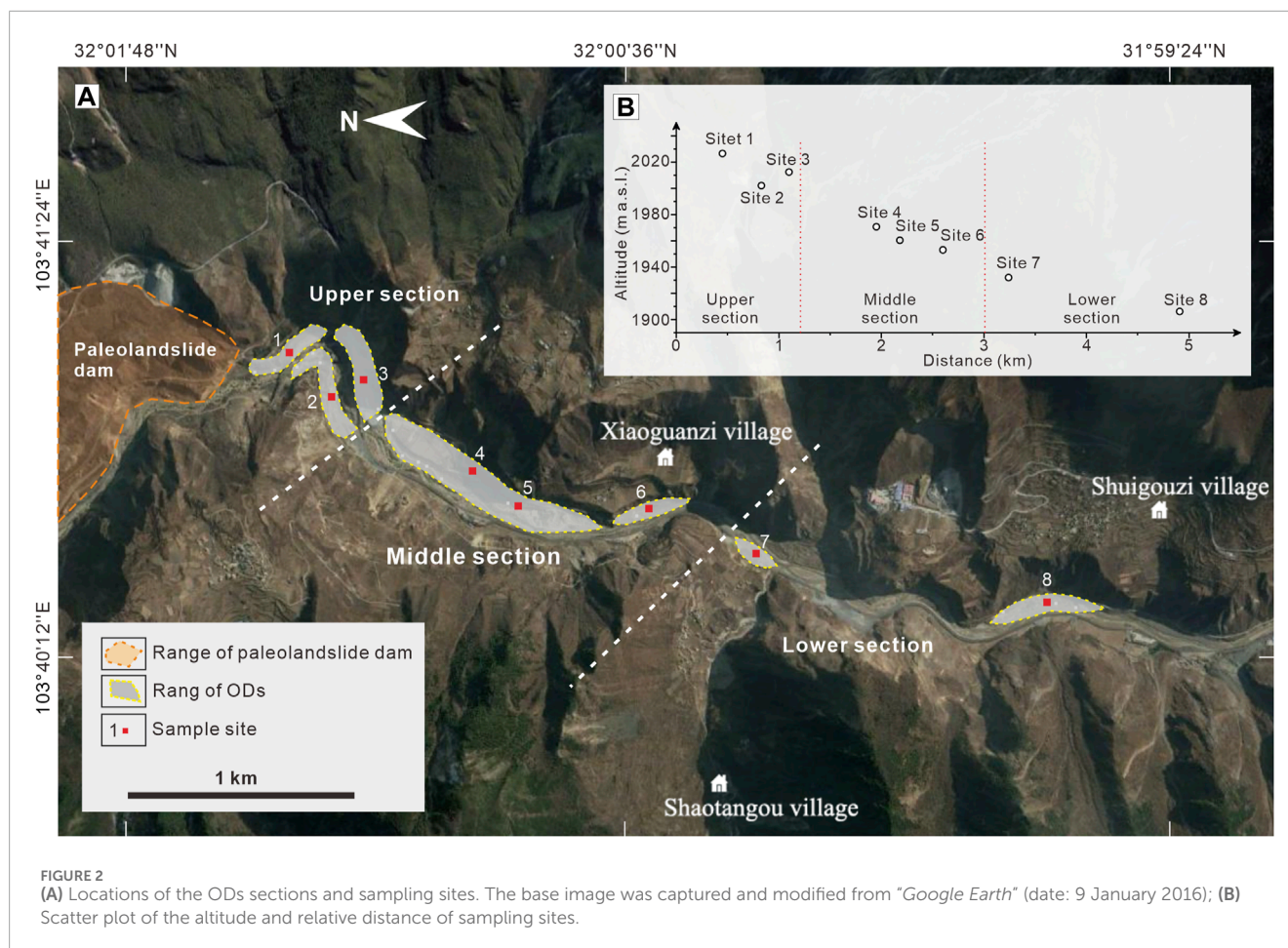


FIGURE 1 Study area. **(A)** Map showing the study area and outline of the active tectonics in the East Tibetan Plateau; **(B)** Lithologies of the exposed bedrocks in the Diexi region of the Upper Minjiang River, and the distribution of the Diexi ancient landslide-dammed lake, lacustrine sections, and ODs (modified from Ma et al. (2022)); **(C)** Topography of the Diexi paleo-landslide area. The base image was captured and modified from "Google Earth" (date: 9 January 2016). The Diexihaizi lakes are modern dammed lakes induced by the Ms. 7.5 Diexi Earthquake that occurred in 1933.



sedimentary structures, to determine the hydrodynamics during the OF stage.

3.2 Sampling

In sedimentology, studying grain size characteristics is the most important aspect of the sedimentary characteristics of clastic sediments. Grain sizes can reflect the transporting dynamic environment and are one of the main characteristics of the deposits. In this study, the ODs distributions in the Diexi Reach of the Upper Minjiang River in the vertical direction were divided into upper, middle, and lower sections (Figure 2). 3 sets of grain size samples were collected from per ODs profile, and each set contained 3 samples from different layers, with approximately 1 kg per sample. A total of 72 grain size samples were collected. Table 1 shows the characteristics of the sampling sites.

3.3 Granularity experiment

The ODs grain size characteristics were tested by laboratory sieving analysis with a set of standard sieves measuring 4, 2, 1, 0.5, 0.25, 0.125, and 0.0625 mm. Then, an arithmetic method of moments is utilized to determine the grain size parameters (mean

particle size, sorting coefficient, skewness, and kurtosis) of the ODs in the study area (McManus, 1988). These are quantitative indicators which effectively reflect the grain-size characteristics and sedimentary environments (Gao and Collins, 1994; Blott and Pye, 2001; Blott and Pye, 2012). Meanwhile, approximately 300 g of fine ODs was collected from per grain size sample for the surface microstructure analysis of quartz sand using a scanning electron microscope (model: Zeiss supra 55). In previous researches, microtextures have been recombined into several microstructure families (Mahaney and Kalm, 2000; Costa et al., 2012; Molén, 2014), which are used to distinguish depositional environments such as desert and glacial sediments (Bellanova et al., 2016). In this study, the comprehensive surface microstructure analysis of ODs quartz sand was performed to classify different characteristics (Immonen, 2013; Chen et al., 2019).

4 Results

4.1 Sedimentary records of landslide-dam breach events

4.1.1 The Diexi Reach in the Upper Minjiang River

In this study, several typical sedimentary and geomorphological features were discovered in the Diexi Reach of the Upper Minjiang

TABLE 1 Descriptions and locations of the ODs sections and sampling sites.

Sampling site	Distance from the relict landslide dam (km)	Exposed length (m)	Maximum thickness (m)	Top elevation (m)	Sample height above channel bottom (m)	Location	
						Latitude/N	Longitude/E
1	0.45	120	9.3	2024.7	8.4	32°01'24.86"	103°41'08.84"
2	0.8	150	25	2032.9	6.0	32°01'20.81"	103°40'57.71"
3	1.2	78	18	2027.2	13.2	32°01'11.38"	103°40'58.11"
4	1.6	25	4.2	1972.8	8.4	32°00'57.56"	103°40'45.00"
5	2.0	110	8.5	1964.3	8.5	32°00'48.91"	103°40'40.22"
6	2.6	60	3.4	1949.4	5.2	32°00'30.36"	103°40'37.12"
7	3.2	30	2.2	1929.2	4.7	32°00'11.77"	103°40'33.35"
8	4.9	62	4.9	1893.5	1.9	31°59'23.22"	103°40'25.27"

River. A relict paleolandslide dam in Jiaochang Village of Diexi Town, lacustrine deposits with a length of approximately 30 km upstream, and an abundance of outburst sediments at approximately 5 km downstream of the Minjiang River were well preserved (Figure 3), indicating that a distinct damming incident had occurred in the Upper Minjiang River that formed a giant paleodammed lake, and that the dammed lake subsequently breached and caused a large OF in the late Pleistocene (Ma et al., 2018).

Eight ODs sections (Table 1) were discovered on both riverbanks at the downstream reach of the Diexi paleo-dam (Figure 4A). The lithology of the exposed ODs are detailed in Figures 4B–I. These deposits present distinctive sedimentary sequences and characteristics. From upstream to downstream, a depositional model in a disordered–sub-ordered–ordered sequence is shown in the distribution of sedimentary profiles. The deposits profile at site 1 (near the breaching gate) are mixed and disordered, without obvious bedding and sedimentary structures (Figure 4B). The gravel in this profile section poorly arranges, with a maximum size of 3.5 m in diameter and “Floating Clasts” characteristics (Russell and Knudsen, 1999; Carling, 2013). The profile and flat surface of the gravel are slightly inclined downstream, with an inclination angle of approximately 7°–9°. Approximately 300 m downstream from the breaching gate, several sedimentary layers appear in the ODs profile, and large boulders are clustered (Figure 4D). Sedimentary layers and bedding characteristics become more obvious in the middle and lower sections than that in the upper section, and a special sedimentary structural unit with a rhythmic interbedding of coarse and fine gravel layers appeared. The bedding is nearly horizontal or slightly inclined downstream. The coarse- and fine-grained layers composed of rhythmic units represent the various “cycles” at site 7 in the lower section (Figure 4H).

These special sedimentary features explain the hydrodynamic changes of the OFs, and are also important indicators for distinguishing the ODs from the other types of sediments in the study area. Some typical “sedimentary facies” units of boulder

(Bcm), coarse gravel (Gm), fine gravel (Gfm), fine sand-gravel (Grm), and sand (St, Sp, and Sh) can be identified from these depositional profiles (Figures 4B–I) and are described as follows:

- Bcm: clast-supported massive coarse boulder gravel layer, with gravel, cobbles, and sand matrix;
- Gm: clast-supported massive coarse gravel layer, with boulders, cobbles, and sand matrix;
- Gfm: massive clast-supported fine gravel layer;
- Grm: massive matrix-supported fine granule-gravel layer;
- St: trough cross-bedded sand layer, with fine gravel;
- Sp: planar cross-bedded sand layer, with fine gravel;
- Sh: massive to thinly laminated medium-coarse sand layer, with fine gravel.

The large boulders in the Bcm units were usually clustered within all of the profiles were laterally extensive, which were approximately horizontal throughout. This unit could be continuously traced between every two profiles, with massive and clast-supported structures. In addition, large numbers of subrounded to rounded boulders were commonly distributed on the riverbed, usually forming ODs terraces, which were mostly covered with bushes and grass, indicating a low water level stage after a high-energy flood flow. The gravel units (Gm, Gfm, and Grm) underlay and overlay the Bcm units, with a lateral expansion from several to tens of meters, which were typically structured by matrix-supported or massive, medium-coarse sandy or silty sand matrices. Sand units (St, Sp, and Sh) were found to exist among the Bcm and gravel units in several sections, forming thin layers or lenses with a maximum thickness of 0.5 m and appearing at different levels. The sand units were horizontally stratified, and contained scattered pebbles.

4.1.2 The Tangjiashan Reach in the Tongkou River

Tangjiashan ODs are distributed from downstream of the landslide dam to Beichuan County, with a length of approximately 5 km (Figure 5). Based on the Google Earth image on 25 December 2015, and field investigations, it was found that the ODs in the reach

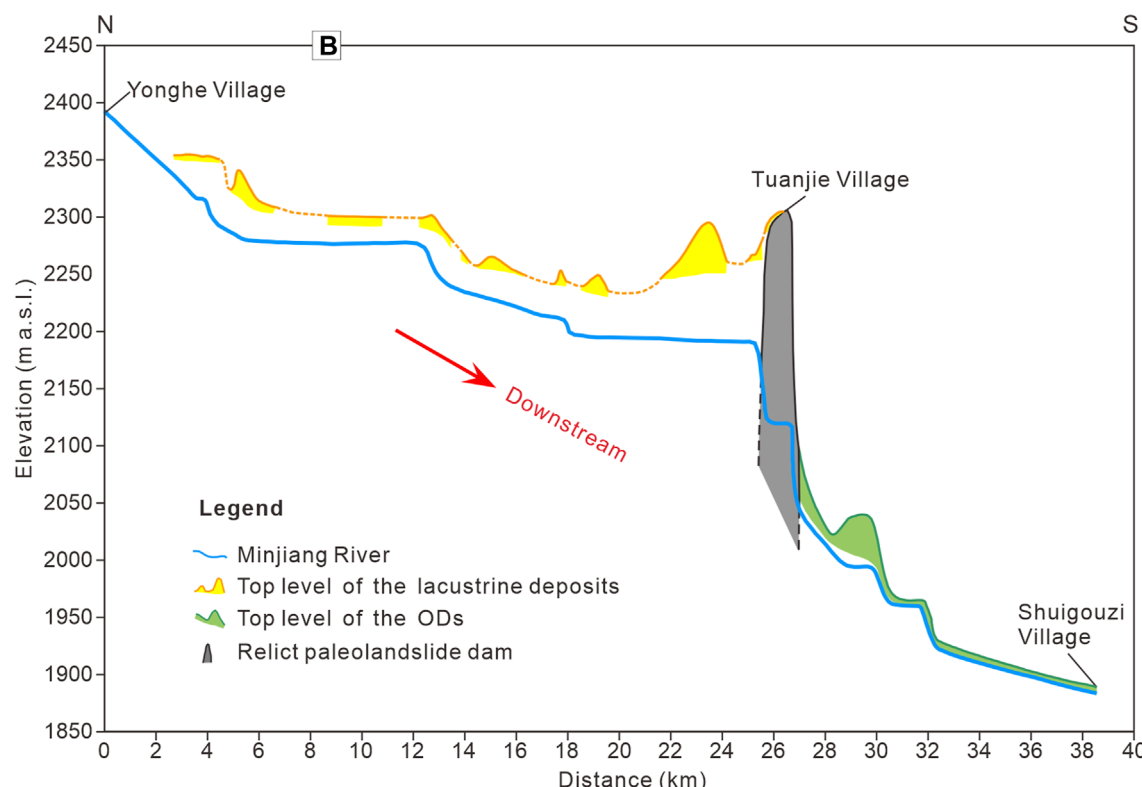
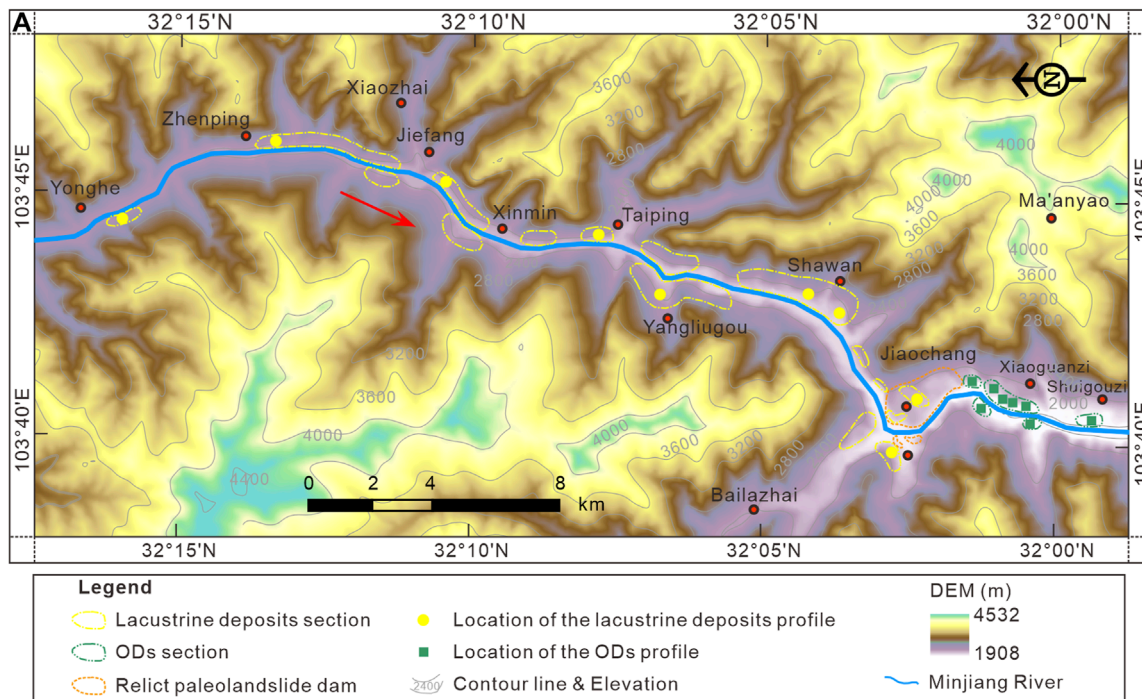


FIGURE 3 Sedimentary geomorphology features in the Diexi Reach of the Upper Minjiang River. (A) Spatial characteristics of sedimentary distribution and topography; (B) Longitudinal profile showing the relict paleolandslide dam in Jiaochang Village of Diexi Town, lacustrine deposits in the upstream, and ODs along the downstream of Minjiang River.

from Tangjiashan to Beichuan can be divided into the upper, middle, and lower sections by the first right turning point of the river channel and the Kuzhuba suspension bridge (Figure 5A). The sedimentary

characteristics of the ODs in the three sections are different and form a corresponding relationship with river channel bending. In addition, there were significant distribution changes in the middle

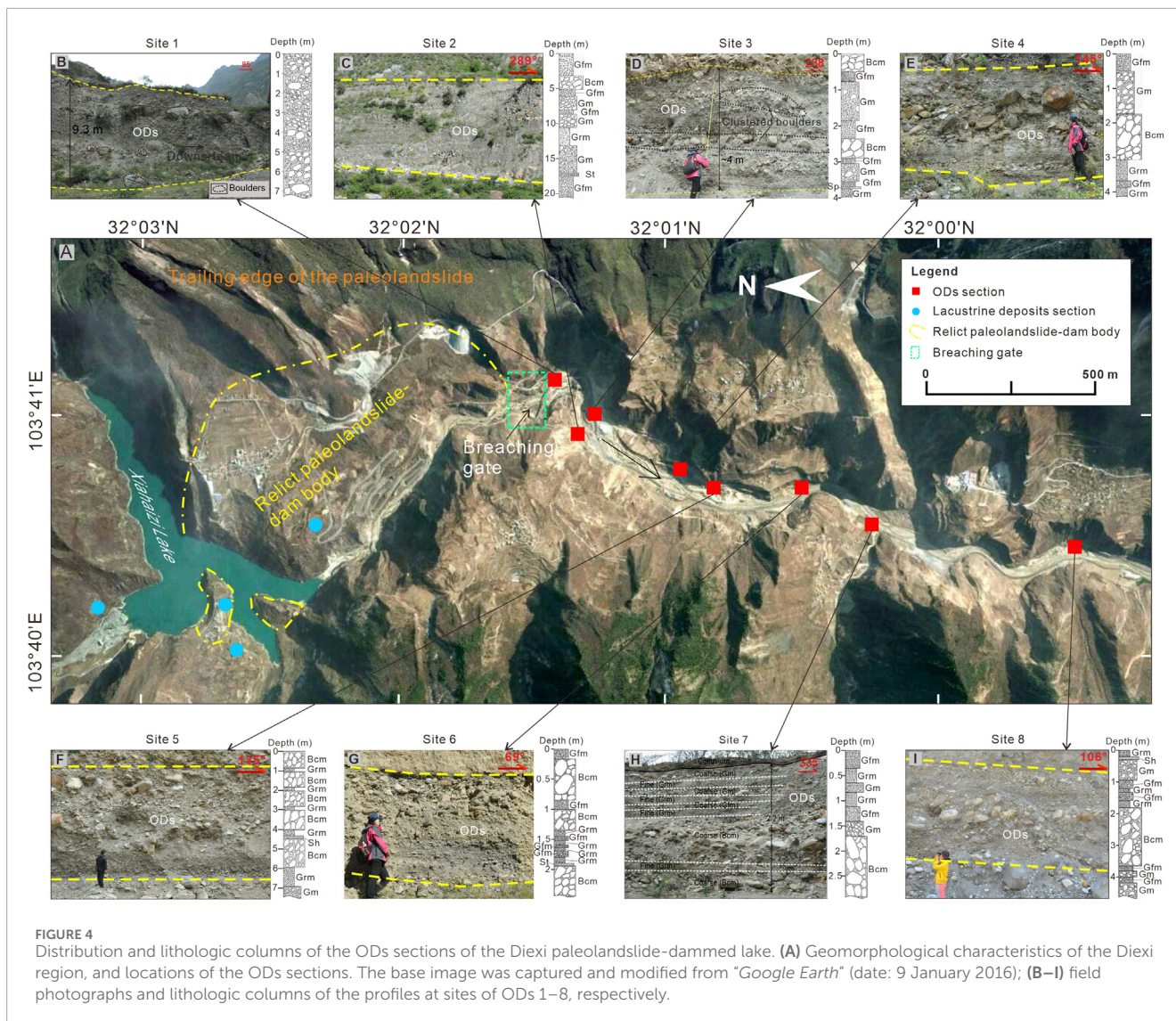


FIGURE 4 Distribution and lithologic columns of the ODs sections of the Dixi paleolandslide-dammed lake. (A) Geomorphological characteristics of the Dixi region, and locations of the ODs sections. The base image was captured and modified from “Google Earth” (date: 9 January 2016); (B–I) field photographs and lithologic columns of the profiles at sites of ODs 1–8, respectively.

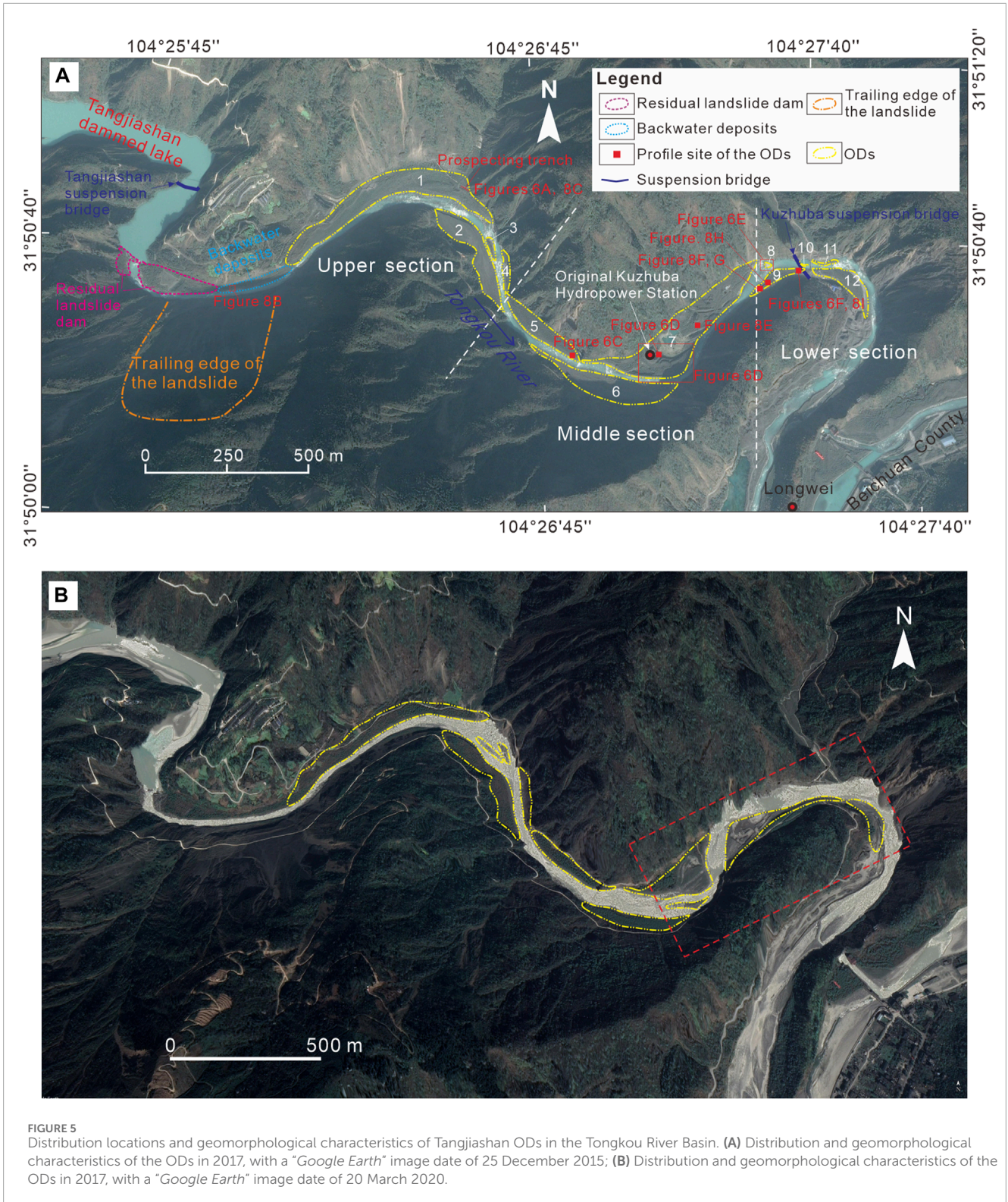
and lower sections of the ODs in the Google Earth image on 20 March 2020 (Figure 5B), which could have been caused by human activities.

The ODs in the upper section (sites 1–4) are distributed in the river valley at a distance of 1.5 km from the landslide dam to the first river bending. Among them, ODs 1 is the largest one, which is distributed in a long strip along the left bank of the river, forming a large platform similar to an “accumulation terrace”. An artificial prospecting trench with a length, width, and height of approximately 5.0, 3.0, and 1.0 m respectively, was explored at the tail of this accumulation profile, and the sedimentary characteristics were clearly visible (Figure 6A). ODs 2 is distributed on the opposite bank (right bank) of the prospecting trench, which is 1.0–2.0 m above the water surface (Figure 6B). Moreover, ODs 3 is pendant-shaped in the river channel, which is small in scale and originally part of ODs 2, separated by river flow cutting.

The middle section of the Tangjiashan ODs is distributed between the first and second major bends of the river channel downstream of the landslide dam, with a length of approximately

2.0 km, including ODs 5–7. The most typical exposed profile in this section is ODs 7 located near the Kuzhuba Hydroelectric Station, which has good continuity and integrity (Figure 5A). The planform of ODs 5 is shuttle shaped, with a prominent vertical exposed profile developed at the end. Although the upper part of the profile is covered by a pile of rubble, a certain arrangement structure can still be recognized (Figure 6C). ODs 6 is distributed on the right bank of the river bend, protruding outward, forming a flat half-moon shape. The fan-shaped ODs 7 extends along the left bank of the river. A typical vertical profile is exposed on the southeast side of the Kuzhuba Hydroelectric Station, with a thickness of approximately 4.0 m and well-developed sedimentary features (Figure 6D). Approximately 200 m upstream of the Kuzhuba suspension bridge at the end of the middle section, gravel content is lower than that of the upper and middle parts, and the gravel size decreases.

ODs 8–12 in the lower section are located at the third river bend downstream of the Tangjiashan landslide dam, with relatively scattered distributions and small scales (Figure 5A). ODs



8, 10, and 12 lie in the river channel, forming gravel diara deposits. These gravel diara are 2.0–3.0 m thick with high gravel content and large gravel (Figure 6E). The presence of gravel diara also indicates that this location is approaching the end of the Tangjiashan ODs. ODs 9 and 12 are the two larger accumulations in the lower section, both of which have a half-moon shape.

Several typical sedimentary structures develop in the profile of ODs 9 (Figure 6F).

The Tangjiashan ODs can be longitudinally divided into five depositional types: erosional residual-dam deposits, backwater deposits, and fan-apex deposits in the upper section; fan-in deposits in the middle section; and fan-margin deposits in the

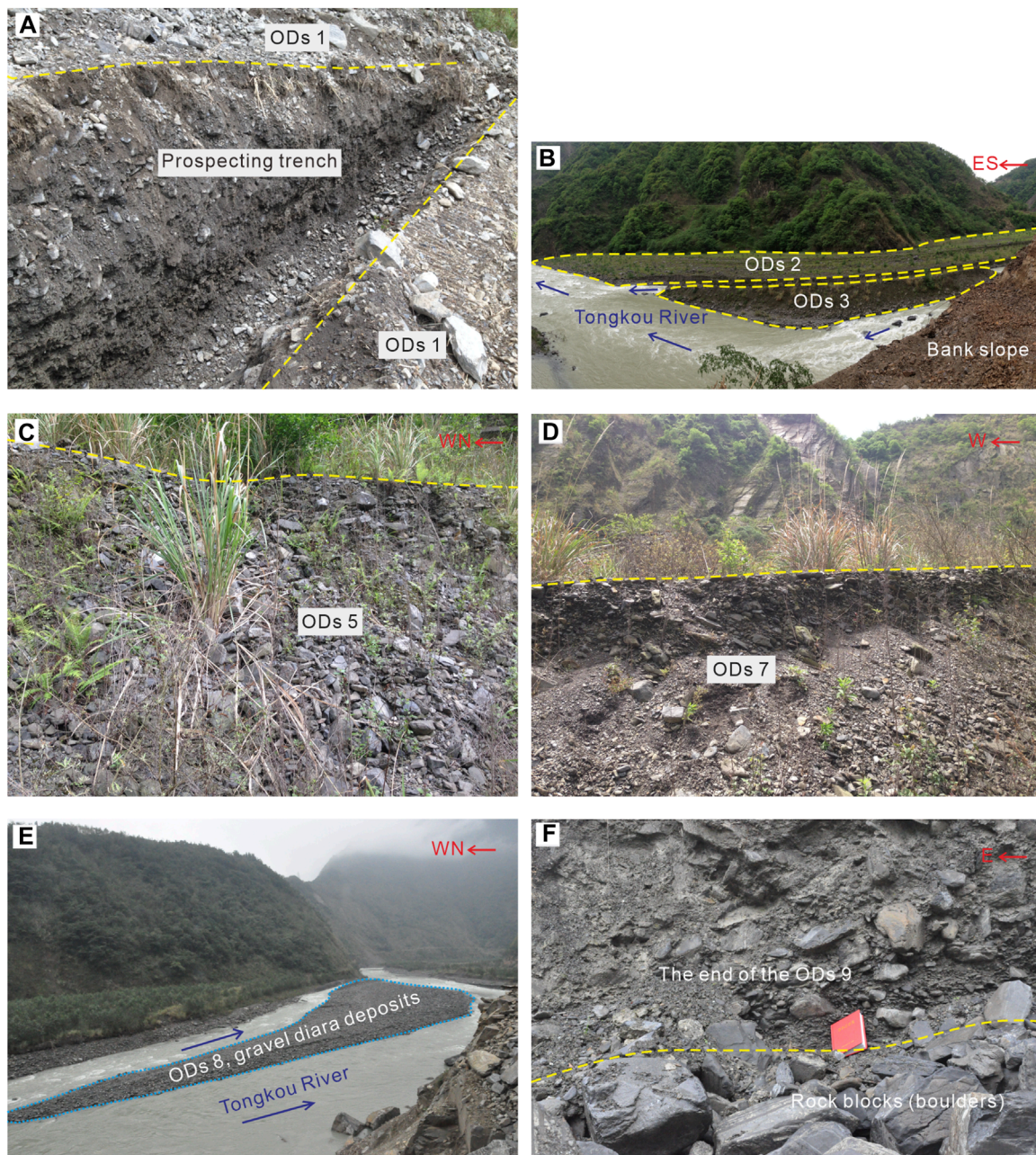


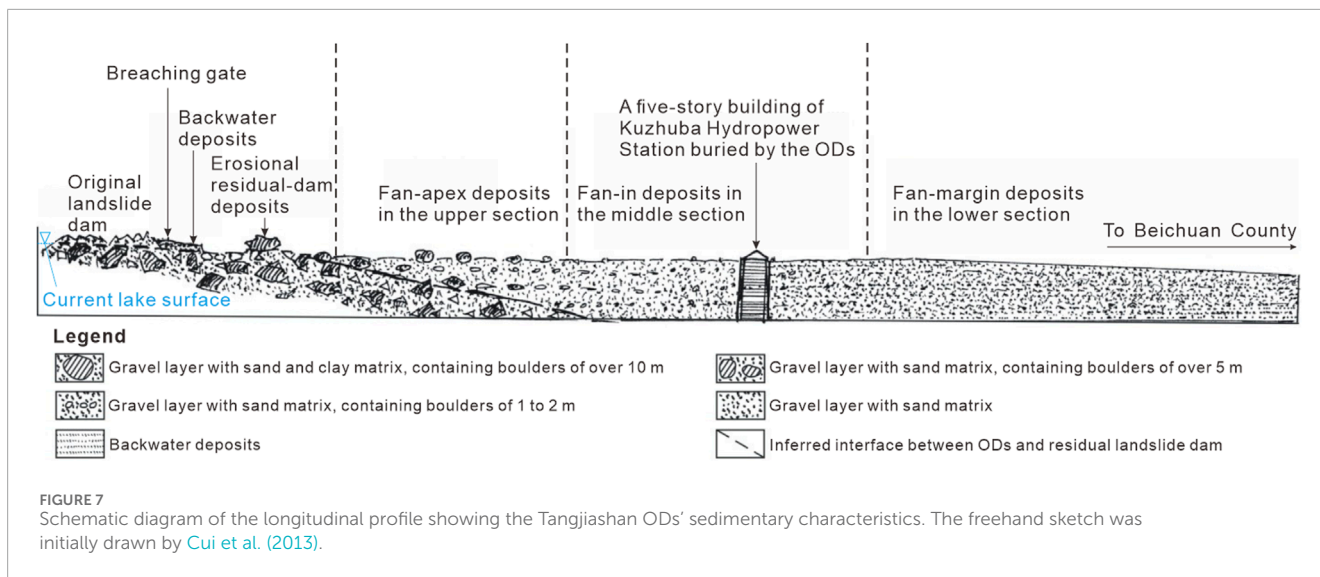
FIGURE 6

Distribution characteristics of Tangjiashan ODs. (A) The artificial trench at the end of ODs 1 in the upper section; (B) The distribution characteristics of ODs 2 and 3 in the upper section; (C) Profile characteristics at the end of ODs 5 in the middle section; (D) Profile characteristics of ODs 7 on the southeast side of the Kuzhuba Power Station in the middle section; (E) Gravel diara deposits in the river center of the lower section; (F) Profile characteristics at the end of ODs 9 in the lower section (See Figure 5 for the locations).

lower section (Figure 7). Six types of sedimentary facies, including Bcm, Gm, Gfm, Grm, and Sp/Sh, are presented in the vertical profiles of the ODs.

The erosional residual-dam deposits is an accumulation unit on the new river channel after lake discharge, which is characterized by several juxtaposed large gravel diara deposits, mainly composed of poorly sorted gravel. In addition, multiple boulders are scattered on the top residual dam, either horizontally on the diara island or in the river channel. The maximum boulder has a particle

size of approximately 8 m and weighs 300 t (Figure 8A). The backwater deposits are composed of sorted sand and fine gravel, with clear horizontal bedding and varying layer thicknesses. The upper and lower parts of the backwater deposits are composed of Grm, and the middle part is composed of multilayer sand faces (St/Sh) (Figure 8B). This is due to the low flood level in the early stage of dam failure, resulting in backflow on both sides of the barrier dam (Figure 5A), which is a sign of early water level drop.



The boulders on the riverbed and diara island of the fan-apex deposits in the upper section, with particle sizes ranging from a few centimeters to several tens of centimeters, are obviously reduced. The exposed profile of the prospecting trench shows typical sedimentary characteristics (Figure 8C). This vertical profile has obvious stratification, but does not have rhythm. The gravel in profile likely formed into imbrication structure characteristics. In addition, the ODs on the diara island and south bank of the river contain few gravel components but more silt. There are loose gravel deposits at the foot of the profile, indicating that the gravel structure in these ODs is unstable and easily scatters under river erosion or gravity.

There are almost no large boulders (particle size >1 m) on the riverbed and diara island in the middle section. A five-story building of the Kuzhuba Hydropower Station buried by the ODs 7. The estimated maximum thickness of the ODs in this section must be more than 15 m (Figure 8D). This also intuitively reflects the water depth of the Tangjiashan LLOFs at the flood stage. Figure 8E shows sedimentary characteristics of an exposed ODs 7 profile on the southeast side of the Kuzhuba Hydropower Station, with clear bedding and structures. There is a clear rhythmic-interbedded structure in the profile horizontal bedding. Five “cycles” could be found in this profile, illustrating that five flood peaks of the LLOF would occur in the dammed-break period. This depositional profile has developed boulder facies (Bcm) and gravel facies (Gm, Gfm and Grm). The coarser gravel layer presents gravel support-stacked, cavitation, stone-in-line and imbrication structures. Clustered gravel in the profile exhibits a “huddling” phenomenon. These sedimentary characteristics explain the regular changes in the hydrodynamic conditions of the OFs at the time of breaching.

The gravel diara on the riverbed of the lower section is mainly composed of fine gravel (<10 cm) and sand. The scale and quantity of gravel diara have increased, resulting in more river bifurcation. Because of the weakening of flood dynamic conditions in the lower section, the pulsating-flow characteristics were also weakened, which makes the stratification characteristics of the ODs indistinct. The exposed profile of ODs 9 in this section presents a combination pattern of an overhead gravel layer at the

lower part, a cemented dense diamicts layer in the upper part, and a slightly inclined bedding layer downstream of the riverbed (Figure 8F). The lower gravel layer of this profile is composed of Gm facies and Bcm facies, with a maximum thickness of 20 cm. Because of the low sand matrix content in the Bcm facies, the gravel in the profile does not have a foundation, forming gravel support-stacked and cavitation structures (Figure 8G). The top part of the ODs 9 profile is a Bcm unit composed of a mixture of large boulders and sand, with a thickness of approximately 50 cm. ODs 9 in the middle section extends to approximately 100 m. It is inferred that the lower Bcm and Gm units should develop in an OF environment with weak hydrodynamic conditions, whereas the upper Bcm unit represents a turbidity-current flood environment with strong hydrodynamic conditions. A similar ODs profile appears approximately 50 m downstream from the above site, with a thickness of only 1.0 m, developing Bcm facies sandwiched with a lens of thin Gfm facies (Figure 8H). Most boulders in the Bcm unit are poorly rounded and disorderly arranged, showing many cavitation structures. These sedimentary characteristics indicate that this profile must have been formed by the rapid accumulation of high-energy OFs, and later eroded by low-energy floods, causing the fine-grained matrix components to be washed away.

Under the Kuzhuba suspension bridge, the sedimentary profile at the end of OFs 9 becomes more mixed (Figure 8I). Only a clearly layered Gfm unit can be distinguished at the bottom of the profile, which is mainly composed of fine gravel and sand without cavitation. The particle size of the boulders distributed in the overlying Bcm unit mostly ranges from 20 to 30 cm and are mainly plate- or sheet-shaped, with poor rounding and mixed arrangement. The sand content of the Gm unit in the upper part of the profile is higher than that of the gravel, and the flat surface of the gravel has an upstream tendency. The profile generally presents disordered sedimentary characteristics, with good cementation, which reflects the fact that when the OF reaches the lower section, its pulsatility becomes weak due to the influence of transmission distance and topography, but it still maintains a strong hydrodynamic condition.

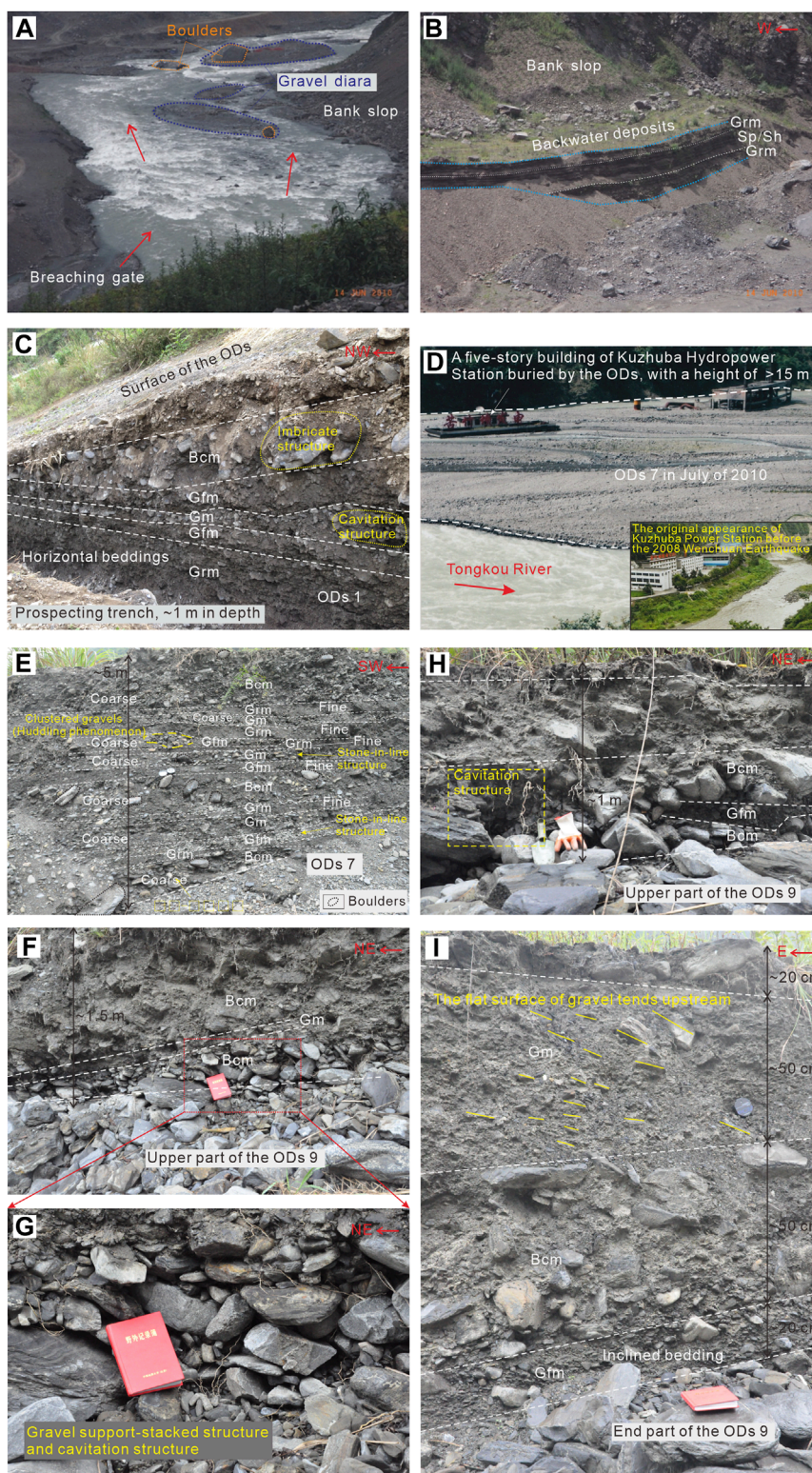


FIGURE 8 Sedimentary characteristics of Tangjiashan ODs. (A) Sedimentary characteristics of residual-dam deposits. The field photo was provided by Cui et al. (2013); (B) Sedimentary characteristics of backwater deposits. The field photo was provided by Cui et al. (2013); (C) Sedimentary characteristics of the prospecting trench at the end of ODs 1 in the upper section; (D) Comparison before and after burring the original Kuzhuba Power Station in the middle section; (E) Sedimentary characteristics of the central part of ODs 7 in the middle section. (F–H) Sedimentary characteristics and structures of the upper part of ODs 9 in the lower section; (I) Sedimentary characteristics of the exposed profile at the end of ODs 9 in the lower section (See Figure 5 for the locations).

TABLE 2 Grain size proportion and sample statistics using the arithmetic moment method of the ODs in the Diexi Reach.

Section	Grain size portion (%)			Sample statistics			
	Gravel (64–2 mm)	Sand (2–0.0625 mm)	Silt and clay (<0.0625 mm)	Mean grain size (mm)	Sorting	Skewness	Kurtosis
Upper	72.01	26.68	1.31	19.57	15.65	0.06	1.42
Middle	70.46	28.04	1.50	18.60	15.91	0.06	1.19
Lower	67.12	30.96	1.92	17.21	16.02	0.06	1.11
Average	69.86	28.56	1.58	18.46	15.81	0.06	1.24

4.2 Grain size characteristics

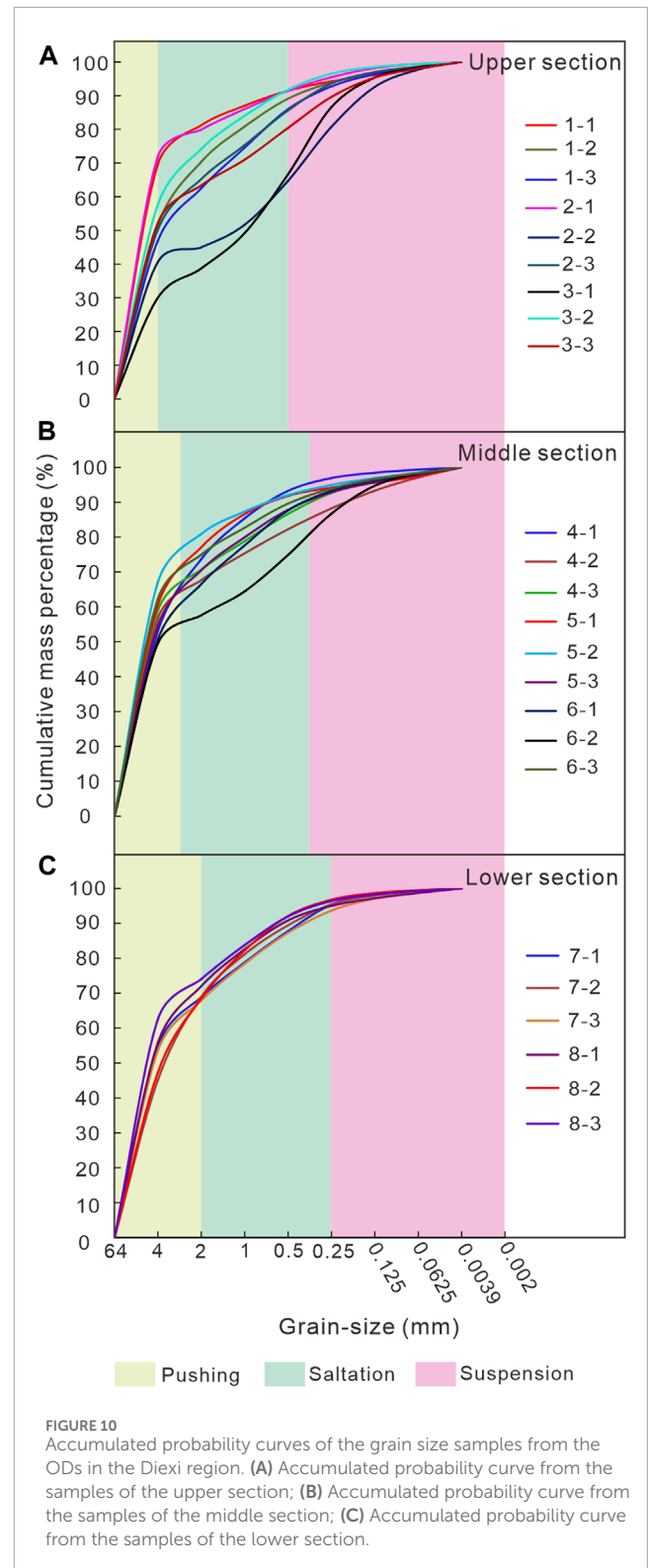
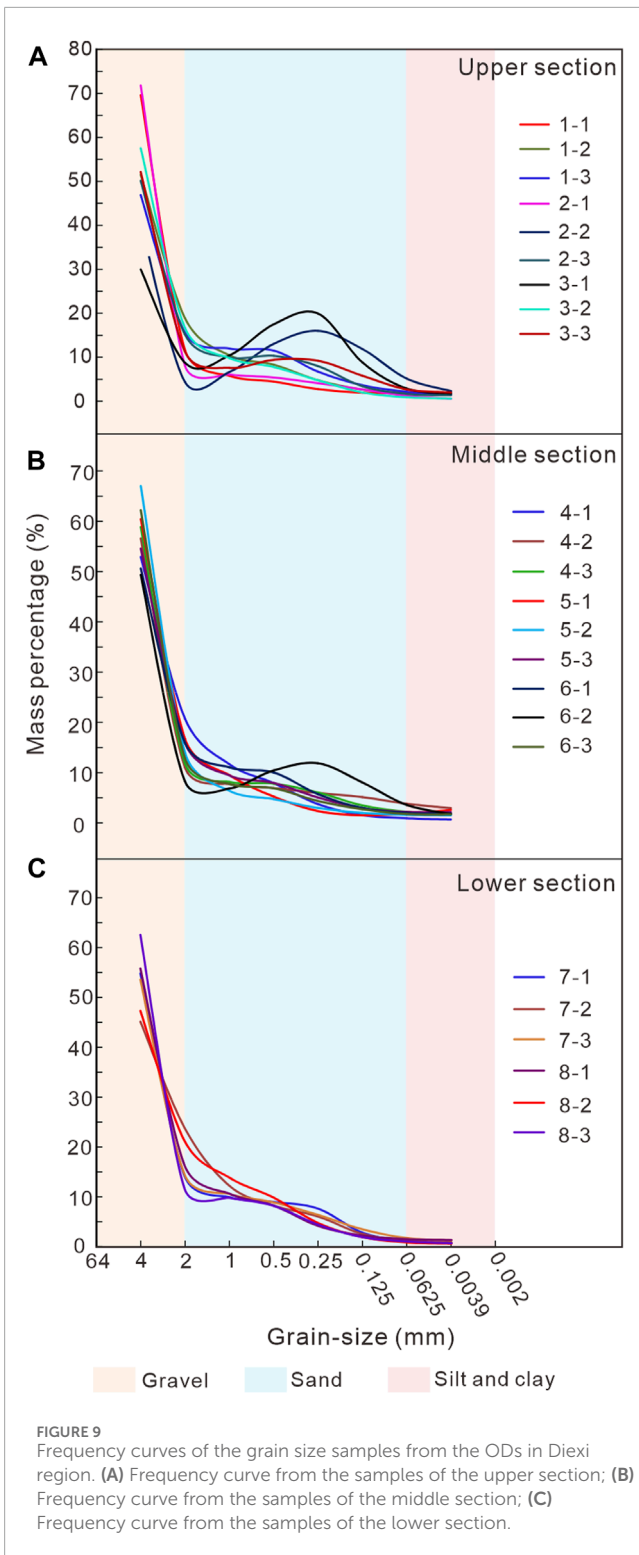
This study determined that the main components (with a particle size of <64 mm) of the ODs in Diexi Reach are gravel (69.86%), followed by sand (28.56%), with minimal content levels of silt and clay (1.58%) (Table 2). Furthermore, from the upper to the lower sections, the gravel content displays a gradual decrease, whereas the sand content increases. The strong hydrodynamics of the OF at the time of dam failure evidently result in rapid deposition of coarse gravel components, while fine-grained components are transported downstream. The fine particles (sand, silt and clay) increased in the middle and lower sections of the ODs, which illustrates that the OF hydrodynamics decreased. The maximum granularity distribution of the ODs occurs at 4 mm, which is the peak of the particle size frequency curve (Figure 9). Furthermore, the large slope of the frequency curve between 4 and 2 mm indicates that the granularity distributes in a small interval and that the particles are relatively concentrated in gravel, which confirms that the OF is in high energy and strong hydrodynamics, resulting in gravel depositing quickly. There is a sub-peak (approximate 0.375 mm) of sand content in the upper section (Figure 9A), but not in the middle and lower sections (Figures 9B,C). However, the particle composition between 2 and 0.0625 mm (sand content) increases from upstream to downstream (Table 2), indicating that the OF energy gradually weakened, and the ODs sorting improved which was similarly characterized to that of the channel sand (Ma et al., 2018). In addition, the transport modes of the ODs in the study area include pushing, saltation, and suspension (Figure 10), which can reflect the material composition, particle sorting, and intersection of transport medium (Visher, 1969). The pushing sections of the grain size accumulated probability curves present steep-slope characteristics, which reflects the material source is coarse-grained detritals, consisting with the fact that the ODs in the study area are mainly composed of gravel components. Furthermore, the curve slopes of the saltation and suspension sections quickly flattened and are much smaller than that of the pushing sections, reflecting a rapid decrease in the content of coarse-grained components from the upper section to the lower section. From upstream to downstream, the intervals of the pushing sections gradually increase, the intervals of the suspension sections gradually decrease, and the interval differences of the saltation sections are small. These findings indicate that the coarser-grain compositions (gravel) decreased and finer-grain compositions (silt

and clay) increased, which resulted from gradually weakened OF energy, stabilized sedimentary environment and, improved sorting from upstream to downstream. In the current study, the grain size characteristics in the upper section of the ODs are similar to those of the debris flow deposits, whereas the grain size characteristics in the middle and lower sections are similar to those of the channel sand sediment. However, with regard to the precise definition of this new type of sedimentary environment, further in-depth study is recommended.

The mean particle-sizes of the upper, middle, and lower segments were 19.57 mm, 18.65 mm, and 17.21 mm, respectively (Figure 11A). From which we may learn that the mean particle-size of the deposits has gradually decreased from the upper section to the lower section. This indicates that a large amount of fine particles have removed by the OF in the upper section, leaving the larger particles behind. The average sorting coefficient values are 15.65, 15.91, and 16.02 for the upper, middle, and lower sections, respectively, with an average sorting coefficient of 15.81, which is characterized by very poor sorting (Figure 11B). However, from the upper section to the lower section, the sorting coefficient value tends to become gradually smaller, which indicates that the sorting of sediment has improved. The average skewness value is 0.06 for each section, which belongs to the symmetrical type (Figure 11C). The deposits presents very coarse skewed-type characteristics, which indicates that the fine particles have easily formed into suspended matter, and then migrated to the lower section by means of pushing and suspension. For the entire study area, the kurtosis values of the sediment ranges between 1.02 and 2.15, with an average value of 1.24. The very platykurtic kurtosis (<1.7) accounts for 91.7%, therefore the ODs in the study area belongs to the very platykurtic type of sediment (Figure 11D). It is determined that the narrower the kurtosis is, the more concentrated the particle-size distribution of the samples would be, which confirms that at least a part of the sedimentary particulates are without environmental modification, and have been directly transformed into the environment in this area.

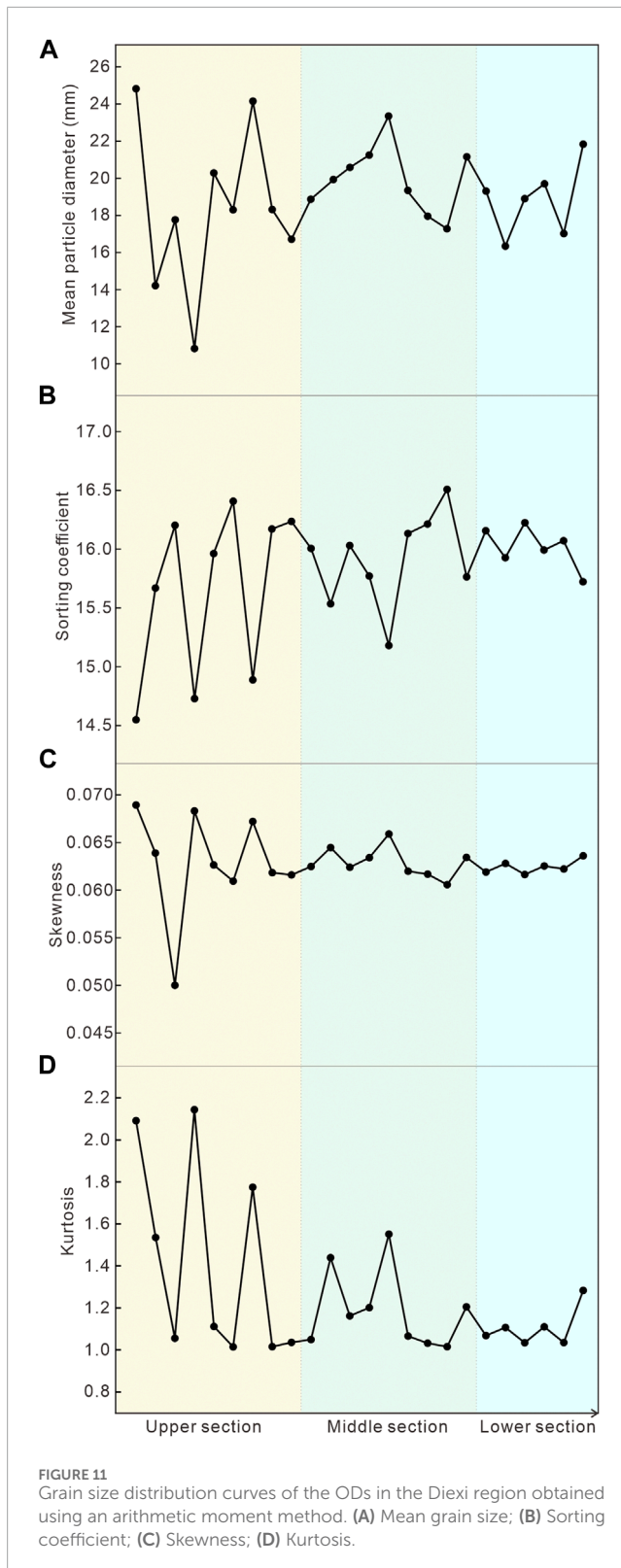
4.3 Surface mechanical microtextures of quartz grain in outburst deposits

The mechanical microtextures of ODs in the Diexi Reach of the Upper Minjiang River, such as fractured plate, conchoidal



fracture, impact crater, and V-shaped pit, are shown in Figure 12. The quartz sand surface of in ODs presents a microtexture of the breakage block with similar large geometry size (Figures 12A,D), which is generated by strong collisions. This type of microtexture characteristic is commonly found in the upper section of the ODs. However, the middle section of the ODs is characterized by conchoidal fracture (Figures 12C,D), which usually occurs in

mineral particles lacking clear joints caused by strong impact (Margolis and Krinsley, 1974; Chen et al., 2019). This study shows that the breakage block frequency in the middle and lower sections of the ODs is arranged from 25% to 33%, which is less than half of that in the upper section. From upstream to downstream, the



frequency of large ($>100\ \mu\text{m}$) and medium ($10\text{--}100\ \mu\text{m}$) conchoidal fractures shows a decreasing trend. However, the frequency of small ($<10\ \mu\text{m}$) conchoidal fractures appearing in the upper and lower sections was higher than that in the middle section. Among them, the upper section has the highest frequency of 40.09% induced by inherited microtextures. The middle and lower sections have small frequencies of conchoidal fractures, with values of

27.83% and 32.08%, respectively, which reflects that the OF energy decreased.

Previous studies indicated that impact crater, V-shaped pit, triangular marks, and impact pit are typical markers observed only in the lower section of the ODs (Figure 12F), whereas impact craters are common in the three sections (Figures 12B–E). However, from the upper section to the lower section of the ODs, the frequency of impact craters did not increase or decrease significantly. In addition, scratch, groove and upturned plate microtextures were also observed in the ODs (Figures 12A–C), with a relatively low percentage of approximately 5.5%. The smooth surface (Figure 12F) with a sparse content of $<6\%$ in the lower section suggests a fast deposition rate at the flood stage.

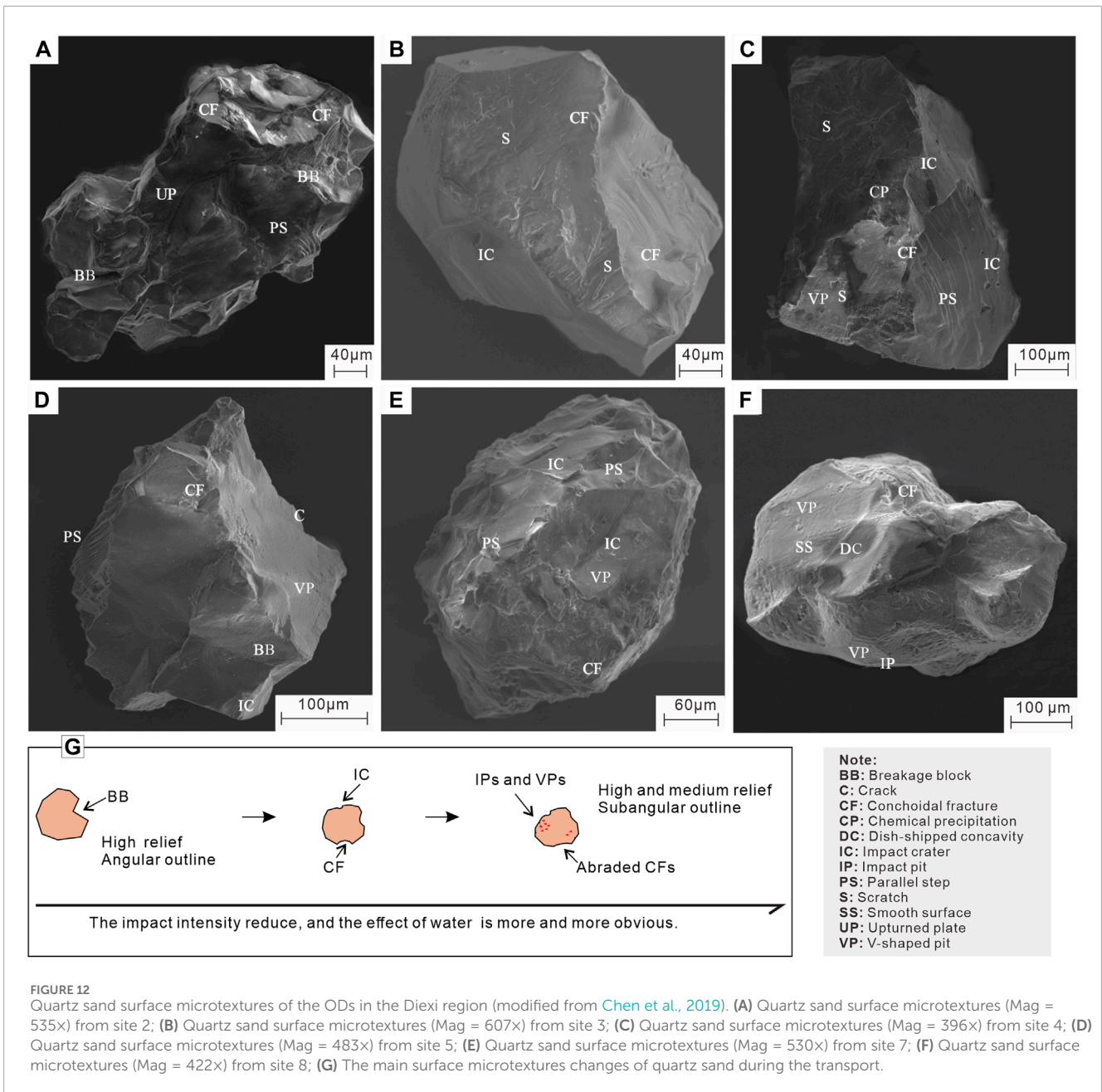
5 Discussion

5.1 Difference between the outburst deposits and other sedimentary types

Overall, the longitudinal distribution of ODs is similar to that of an elongated fan-shaped terrace along the river channel (Figure 13). Based on the morphological characteristics and developmental locations, ODs can generally be divided into upper, middle and lower sections from upstream to downstream, which presents an obvious development regulation and distinctive sedimentary characteristics.

From the perspective of developmental characteristics, the sedimentary sequences of the ODs are between alluvial and debris flow facies (Bridge, 1984; Blair and McPherson, 1998; Moscariello et al., 2002; Ferring, 2020; Miall, 2022). The graded bedding texture in ODs is clearer than that in debris flow deposits, but there is no reverse or positive bedding rhythm in alluvial deposits. With regard to the macroscopic characteristics, the ODs profiles exhibit the accumulation characteristics of normal fluvial deposits, such as a large-scale rough sorting mechanism (Bridge, 2006; Dino et al., 2012; Miall, 2013). Meanwhile, on a microscopic level, they also exhibit the characteristics of diluted debris flow deposits (Eyles et al., 1988; Sohn et al., 1999), such as mixed sizes of gravel fragments and extremely inhomogeneous particle sizes, which reflects a rapid and erratic accumulation process (Ma et al., 2018). In terms of sediment formation conditions and distribution, ODs are also different from alluvial and debris flow deposits. On the one hand, regardless of the scale or flow magnitude of the material source, the formation conditions of ODs far exceed those of fluvial deposits, which also results in the absence of rhythmic characteristics of fluvial deposits in the ODs. On the other hand, the ODs lack the ability to maintain integrity such as debris flow deposits, which will still be affected by river transformation in the later stage. In addition, the ODs' surface is flat and has a long extension, with a leading front edge angle generally below 30° , which is different from the sharp-surface sedimentary facies of alluvial deposits and the large-angle front edge of debris flow deposits (Blair and McPherson, 1994; Bernhardt et al., 2012; Alván and von Eynatten, 2014; Chen et al., 2017).

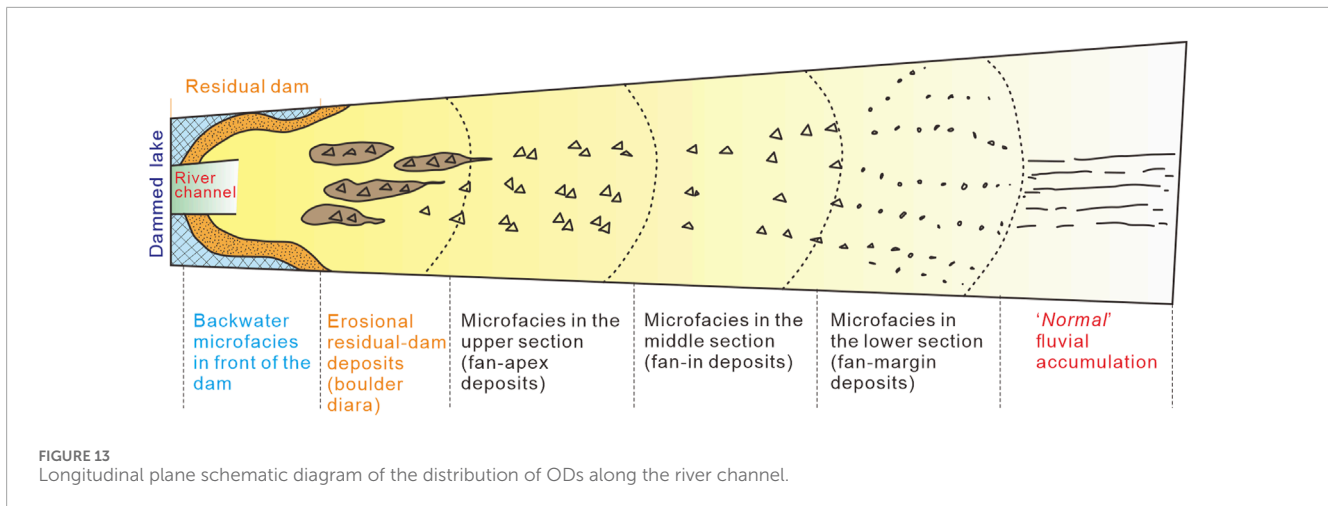
In the microcosmic research of sediments, quartz sand surface microtextures have been widely applied in the reconstruction of sedimentary environments (Sweet and Soreghan, 2010; Vos et al.,



2014; Gobala krishnan et al., 2015). Based on the statistical results of quartz grain surface microtextures in ODs, it indicates that the combination of mechanical microtextures changes obviously along the transporting distance of the ODs (Chen et al., 2019). Near the breaching gate, the morphology of quartz grains is controlled by the breakage blocks, which is similar to the grains of colluvial deposits (Goudie and Bull, 1984). However, the inherited microtextural features (e.g., fluvial sediments, lacustrine sediments and landslide deposits) representing these morphological modifications are uneven, which may be related to the high concentrations and rapid deposit process. As the distance increases, the quartz grains in the ODs become more similar to the grains from debris flow (Deane, 2010), which are characterized by medium conchoidal fractures and impact craters. In addition, the roundness

of quartz sands and frequent V-shaped pits and impact pits also improved with transporting distance (Figure 12G). The different combinations of quartz sand surface textures indicated that the transformation process changed from high energy collisions to low energy collisions over a short distance, which was controlled by the hydrodynamic conditions or flow regime (Chen et al., 2019).

In sedimentology, based on sedimentary bedding and sorting degree, the sedimentary types can generally be divided into ordered and disordered, or ordered, sub-ordered, and disordered, and any sedimentary type can only possess one sedimentary sequence (Harms et al., 1975; Reading, 2009; Cui et al., 2013; Miall, 2022). Nevertheless, due to the influence of dynamic and medium composition changes during transportation and accumulation, the ODs will form disordered sedimentary sequence in the upper



section, whereas sub-ordered or ordered sedimentary sequences will form in the middle and lower sections. It is completely absent in sedimentary deposits (Ma et al., 2018).

5.2 Different characteristics of the landslide-dammed lake outburst floods from “normal” floods

In a “normal” flood stage, low discharge and intensity are consistent throughout the entire basin, which should form similar sedimentary characteristics in sediments (McKee et al., 1967; Mutti et al., 2000; Wang et al., 2023a). However, the ODs exhibited inconsistent characteristics in the deposits profiles. Near the breaching gate, the OF is under large-discharge and high-energy, thus forming disorganized deposits profiles with no obvious beddings, which are similar to the characteristics of “normal” flood accumulation. In addition, the gravel in these profiles is disordered and mixed with some isolated boulders. Subsequently, with an increase in the transporting distance, the OF discharge and intensity decreased gradually, and the regularity of sedimentary characteristics also gradually became observable, such as the increasingly obvious stratification characteristics and the gradual reduction of gravel particle size.

Different sedimentary units in the ODs profiles record contrasting transportation mechanisms. The characteristics of massive and clast-supported structures, gravel cavitation, no or poor sorting, and profile thicknesses in the Bcm unit indicate that its formation conditions are closely related to high-energy flow (Smith, 1986; Maizels, 1997; Cutler et al., 2002). This is consistent with the transporting and sedimentation characteristics of OFs, speculating that they should be accumulated by OFs. Gm, Gfm, and Grm represent the recession stage of ODs, whereas the thin-layer Sh, St, and Sp represent a brief sedimentary period under stable weak hydrodynamic conditions after the accumulation of boulder units within the same flood peak “cycle”. The isolated boulders in deposits profiles are transported and rapidly deposited by high-energy flood flows (Russell and Knudsen, 2002), which provides strong evidence of LLOFs. In addition, because of the high flow velocity and transport energy of the OF, most of the fine-grained components

cannot be quickly deposited but are transported downstream for a longer distance. Therefore, no extremely fine sand and clay units were found in the ODs.

5.3 Reconstruction of catastrophic paleo landslide-dammed lake outburst floods

According to the statistics of large floods recorded worldwide in a previous research, the OFs caused by ice or landslide dams are much larger than that caused by rainstorms (O'Connor and Costa, 2004; Benito and Thorndycraft, 2020), and its erosive geomorphology, sedimentation process, flood magnitude, and flooding path have distinct temporal and spatial characteristics (Baker et al., 1993; Carling, 2013). The reconstruction of catastrophic paleo LLOFs is conducted on the basis of accurate identification of geomorphological evidence and chronology. The geomorphological map was completed along the flooding path during the same period as the catastrophic paleo OFs. Then, flood level indicators within ODs are identified by comparing and analyzing the evidence of different types of paleo-flood topography (O'Connor et al., 2022; Guo et al., 2023).

Hydraulic models for catastrophic paleoflood reconstruction mainly have two types: stable and unstable. The calculation of the flow surface profile in the stable hydraulic model assumes that the geomorphological indicators of the paleoflood are in close proximity to the maximum flood water level. However, it is crucial to determine the water level and flow rate of the OF in the unsteady simulating hydraulic model. In addition, the flow discharge of the OFs also depends on the water elevation and volume of the dammed lake and the breaching gate and cross-section geometry. On the basis of the sensitivity assessment between geomorphological evidence and water surface elevation changes of the OFs, the simulating model's validation was conducted (Baker et al., 1993; Carling, 2013; Benito and Thorndycraft, 2020; Benito et al., 2023). In terms of high-energy floods, such as OFs or flash floods in mountain regions, flow or boulder competence methods are applicable to estimate the hydraulics of floods using the relationships between the energy parameters of the flow and the geometric characteristics of the sediment particles being transported

by the floods (Costa, 1983; O'Connor, 1993; Ma et al., 2022). Because of the significant uncertainty of hydraulic parameters used in these empirical formulas, it is necessary to verify the rationality of calculating the results in combination with other geomorphological evidence and models (Wohl, 1992; Greenbaum et al., 2020; Ma et al., 2022). Therefore, detecting the estimated results of discharge and evaluating the topographic changes caused by OFs is important in the reconstruction of catastrophic paleo-OFs.

6 Conclusion

During the evolution of LLOFs, materials from the landslide dam and bank slopes and riverbed are transported downstream and gradually deposited, forming ODs in the river channel. This phenomenon is particularly common in some ancient landslide-dammed lakes. This study discovered the development of large-scale ODs in the Diexi Reach of the Upper Minjiang River, and thus obtained a preliminary understanding of ancient giant ODs and LLOFs. Investigations and studies were also conducted on Tangjiashan ODs. These have become important means of studying giant landslide-dam breach events. The accumulation profile has developed structural features such as imbrication, cavitation, gravel support stacking, and rhythmic interbedding. Moreover, the ODs possess some typical “*sedimentary facies*” Bcm, Gm, Gfm, Grm, and sand (St, Sp, and Sh). Among them, the Bcm units are deposited by high-energy OF events, and the gravel and sand units represent the recession stage of the flood.

This study determined that the main components (with a particle size of <64 mm) of the ODs in Diexi Reach are gravel, followed by sand, with minimal content levels of silt and clay, which mainly originate from the landslide dam. From the upper to the lower sections, the coarser-grain compositions (gravel) decreased and finer-grain compositions (silt and clay) increased, which resulted from gradually weakened OF energy, stabilized sedimentary environment and, improved sorting from upstream to downstream. The mean particle-size and sorting of the ODs all displays gradual decreases from the upper section to the lower section, which indicates that the sorting of ODs tends to improve. There is found to be a tendency for the skewness to become larger from the upstream to the downstream, and the ODs presents a very coarse skewed type. The kurtosis of the ODs is distributed in all of the types. The narrower the kurtosis is, the more concentrated the particle-size distribution of the samples would be, which indicates that at least a portion of the sedimentary particulates is without environmental modification, and is directly transformed into the environment. In addition, the different combinations of quartz sand surface microtextures indicate the transformation from high-to low-energy impacts over a short distance, which is controlled by flood hydrodynamics and regime.

Overall, the longitudinal distribution of ODs is similar to that of an elongated fan-shaped terrace along the river channel. Disordered sedimentary sequences are formed in the upper section, whereas sub-ordered or ordered sedimentary sequences are formed in the middle and lower sections, which are completely absent in sedimentary deposits. The sedimentary sequences of the ODs lie between the alluvial and debris flow facies. The

graded bedding texture in ODs is clearer than that in debris flow deposits, but there is no reverse or positive bedding rhythm in alluvial deposits. With regard to the macroscopic characteristics, the ODs profiles exhibit accumulation characteristics of normal fluvial deposits. Meanwhile, on a microscopic level, they also exhibit the characteristics of diluted debris flow deposits.

The special sedimentary characteristics of ODs can explain the hydrodynamic changes during the propagation of OFs and are important indicators for distinguishing between ODs and “*normal*” floods.

Data availability statement

The raw data supporting the conclusion of this article will be made available by the authors, without undue reservation.

Author contributions

JM: Conceptualization, Data curation, Formal Analysis, Investigation, Methodology, Software, Supervision, Validation, Visualization, Writing–original draft, Writing–review and editing. JC: Data curation, Investigation, Methodology, Project administration, Supervision, Validation, Writing–review and editing. CX: Conceptualization, Formal Analysis, Funding acquisition, Project administration, Resources, Software, Supervision, Writing–original draft.

Funding

The author(s) declare that financial support was received for the research, authorship, and/or publication of this article. This research study was supported by the National Institute of Natural Hazards, Ministry of Emergency Management of China (Grant no. 2023-JBKY-57).

Conflict of interest

The authors declare that the research was conducted in the absence of any commercial or financial relationships that could be construed as a potential conflict of interest.

The author(s) declared that they were an editorial board member of Frontiers, at the time of submission. This had no impact on the peer review process and the final decision.

Publisher's note

All claims expressed in this article are solely those of the authors and do not necessarily represent those of their affiliated organizations, or those of the publisher, the editors and the reviewers. Any product that may be evaluated in this article, or claim that may be made by its manufacturer, is not guaranteed or endorsed by the publisher.

References

- Alván, A., and von Eynatten, H. (2014). Sedimentary facies and stratigraphic architecture in coarse-grained deltas: anatomy of the Cenozoic Camaná Formation, southern Peru (16°25'S to 17°15'S). *J. S. Am. Earth Sci.* 54, 82–108. doi:10.1016/j.jsames.2014.04.008
- Baker, V. R. (2008). Paleoflood hydrology: origin, progress, prospects. *Geomorphology* 101 (1–2), 1–13. doi:10.1016/j.geomorph.2008.05.016
- Baker, V. R., Benito, G., Brown, A. G., Carling, P. A., Enzel, Y., Greenbaum, N., et al. (2022). Fluvial palaeohydrology in the 21st century and beyond. *Earth Surf. Process. Landforms* 47 (1), 58–81. doi:10.1002/esp.5275
- Baker, V. R., Benito, G., and Rudoy, A. N. (1993). Paleohydrology of late Pleistocene superflooding, alтай mountains, siberia. *Science* 259 (5093), 348–350. doi:10.1126/science.259.5093.348
- Baker, V. R., and Carling, P. A. (2022). “6.38 - global late quaternary megafloods,” in *Treatise on geomorphology*. Editor J. F. Shroder Second edition (San Diego: Academic Press), 832–840.
- Bazai, N. A., Cui, P., Carling, P. A., Wang, H., Hassan, J., Liu, D., et al. (2021). Increasing glacial lake outburst flood hazard in response to surge glaciers in the Karakoram. *Earth-Science Rev.* 212, 103432. doi:10.1016/j.earscirev.2020.103432
- Bellanova, P., Bahlburg, H., Nentwig, V., and Spiske, M. (2016). Microtextural analysis of quartz grains of tsunami and non-tsunami deposits – a case study from Tirúa (Chile). *Sediment. Geol.* 343, 72–84. doi:10.1016/j.sedgeo.2016.08.001
- Benito, G., Ballesteros-Cánovas, J. A., and Díez-Herrero, A. (2023). “Chapter 2 - paleoflood hydrology: reconstructing rare events and extreme flood discharges,” in *Hydro-meteorological hazards, risks, and disasters*. Editors J. F. Shroder, P. Paron, and G. D. Baldassarre Second Edition (Boston: Elsevier), 33–83.
- Benito, G., Harden, T. M., and O'Connor, J. (2022). “6.35 - quantitative paleoflood hydrology,” in *Treatise on geomorphology*. Editor J. F. Shroder Second Edition (Oxford: Academic Press), 743–764.
- Benito, G., Macklin, M. G., Panin, A., Rossato, S., Fontana, A., Jones, A. F., et al. (2015). Recurring flood distribution patterns related to short-term Holocene climatic variability. *Sci. Rep.* 5, 16398. doi:10.1038/srep16398
- Benito, G., Sánchez-Moya, Y., and Sopena, A. (2003). Sedimentology of high-stage flood deposits of the Tagus River, Central Spain. *Sediment. Geol.* 157 (1–2), 107–132. doi:10.1016/S0037-0738(02)00196-3
- Benito, G., and Thorndycraft, V. R. (2020). Catastrophic glacial-lake outburst flooding of the patagonian ice sheet. *Earth-Science Rev.* 200, 102996. doi:10.1016/j.earscirev.2019.102996
- Bernhardt, A., Stright, L., and Lowe, D. R. (2012). Channelized debris-flow deposits and their impact on turbidity currents: the Puchkirchen axial channel belt in the Austrian Molasse Basin. *Sedimentology* 59 (7), 2042–2070. doi:10.1111/j.1365-3091.2012.01334.x
- Blair, T. C., and McPherson, J. G. (1994). Alluvial fans and their natural distinction from rivers based on morphology, hydraulic processes, sedimentary processes, and facies assemblages. *J. Sediment. Res.* 64 (3a), 450–489. doi:10.1306/D4267DDE-2B26-11D7-8648000102C1865D
- Blair, T. C., and McPherson, J. G. (1998). Recent debris-flow processes and resultant form and facies of the Dolomite alluvial fan, Owens Valley, California. *J. Sediment. Res.* 68 (5), 800–818. doi:10.2110/jsr.68.800
- Blott, S. J., and Pye, K. (2001). GRADISTAT: a grain size distribution and statistics package for the analysis of unconsolidated sediments. *Earth Surf. Process. Landf.* 26 (11), 1237–1248. doi:10.1002/esp.261
- Blott, S. J., and Pye, K. (2012). Particle size scales and classification of sediment types based on particle size distributions: Review and recommended procedures. *Sedimentology* 59 (7), 2071–2096. doi:10.1111/j.1365-3091.2012.01335.x
- Bo, W., Zhang, T., Qin, Z., Chao, W., Chen, Y.-L., and Ping, W. (2015). A case study of the Tangjiashan landslide dam-break. *J. Hydrodynamics, Ser. B* 27 (2), 223–233. doi:10.1016/S1001-6058(15)60476-0
- Borghain, B., Mathew, G., Chauhan, N., Jain, V., and Singhvi, A. K. (2020). Evidence of episodically accelerated denudation on the Namche Barwa massif (Eastern Himalayan syntaxis) by megafloods. *Quat. Sci. Rev.* 245, 106410. doi:10.1016/j.quascirev.2020.106410
- Bridge, J. S. (1984). Large-scale facies sequences in alluvial overbank environments. *J. Sediment. Res.* 54 (2), 583–588. doi:10.1306/212F8477-2B24-11D7-8648000102C1865D
- Bridge, J. S. (2006). “Fluvial facies models: recent developments,” in *Facies models revisited*. Editors H. W. Posamentier, and R. G. Walker (McLean, VA: SEPM Society for Sedimentary Geology), 1–17.
- Burchfiel, B. C., Zhiliang, C., Yupinc, L., and Royden, L. H. (1995). Tectonics of the longmen Shan and adjacent regions, Central China. *Int. Geol. Rev.* 37 (8), 661–735. doi:10.1080/00206819509465424
- Carling, P. A. (2013). Freshwater megaflood sedimentation: what can we learn about generic processes? *Earth-Science Rev.* 125, 87–113. doi:10.1016/j.earscirev.2013.06.002
- Chang, D. S., and Zhang, L. M. (2010). Simulation of the erosion process of landslide dams due to overtopping considering variations in soil erodibility along depth. *Nat. Hazards Earth Syst. Sci.* 10 (4), 933–946. doi:10.5194/nhess-10-933-2010
- Chen, J., Dai, F., Lv, T., and Cui, Z. (2013). Holocene landslide-dammed lake deposits in the Upper Jinsha River, SE Tibetan Plateau and their ages. *Quat. Int.* 298, 107–113. doi:10.1016/j.quaint.2012.09.018
- Chen, J., Zhou, W., Cui, Z., Li, W., Wu, S., and Ma, J. (2018). Formation process of a large paleolandslide-dammed lake at Xuelongnang in the upper Jinsha River, SE Tibetan Plateau: constraints from OSL and 14 C dating. *Landslides* 15, 2399–2412. doi:10.1007/s10346-018-1056-3
- Chen, L., Steel, R. J., Guo, F., Olariu, C., and Gong, C. (2017). Alluvial fan facies of the yongchong basin: implications for tectonic and paleoclimatic changes during late cretaceous in SE China. *J. Asian Earth Sci.* 134, 37–54. doi:10.1016/j.jseas.2016.10.010
- Chen, R., Chen, J., Ma, J., and Cui, Z. (2019). Quartz grain surface microtextures of dam-break flood deposits from a landslide-dammed lake: a case study. *Sediment. Geol.* 383, 238–247. doi:10.1016/j.sedgeo.2019.02.010
- Chen, Z., Ma, L., Yu, S., Chen, S., Zhou, X., Sun, P., et al. (2015). Back analysis of the draining process of the Tangjiashan barrier lake. *J. Hydraulic Eng.* 141 (4), 05014011. doi:10.1061/(asce)hy.1943-7900.0000965
- Costa, J. E. (1983). Paleohydraulic reconstruction of flash-flood peaks from boulder deposits in the Colorado Front Range. *Geol. Soc. Am. Bull.* 94 (8), 986–1004. doi:10.1130/0016-7606(1983)94<986:PROFPF>2.0.CO;2
- Costa, J. E., and Schuster, R. L. (1988). The formation and failure of natural dams. *Geology Soc. Am. Bull.* 100 (7), 1054–1068. doi:10.1130/0016-7606(1988)100<1054:TFAFON>2.3.CO;2
- Costa, P. J. M., Andrade, C., Dawson, A. G., Mahaney, W. C., Freitas, M. C., Paris, R., et al. (2012). Microtextural characteristics of quartz grains transported and deposited by tsunamis and storms. *Sediment. Geol.* 275, 55–69. doi:10.1016/j.sedgeo.2012.07.013
- Cui, P., Dang, C., Zhuang, J., You, Y., Chen, X., and Scott, K. M. (2012). Landslide-dammed lake at Tangjiashan, Sichuan Province, China (triggered by the Wenchuan Earthquake, May 12, 2008): risk assessment, mitigation strategy, and lessons learned. *Environ. Earth Sci.* 65 (4), 1055–1065. doi:10.1007/s12665-010-0749-2
- Cui, Z., Ge, D., Guan, B., Li, D., Zhang, X., Chen, J., et al. (2013). *Diamicts and environment*. Shijiazhuang, China: Hebei Science and Technology Press.
- Cutler, P. M., Colgan, P. M., and Mickelson, D. M. (2002). Sedimentologic evidence for outburst floods from the Laurentide Ice Sheet margin in Wisconsin, USA: implications for tunnel-channel formation. *Quat. Int.* 90 (1), 23–40. doi:10.1016/S1040-6182(01)00090-8
- Dai, F. C., Lee, C. F., Deng, J. H., and Tham, L. G. (2005). The 1786 earthquake-triggered landslide dam and subsequent dam-break flood on the Dadu River, southwestern China. *Geomorphology* 65 (3–4), 205–221. doi:10.1016/j.geomorph.2004.08.011
- Deane, S. M. (2010). *Quartz grain microtextures and sediment provenance: using scanning electron microscopy to characterize tropical highland sediments from costa rica and the dominican republic*. Master of Science (Knoxville: University of Tennessee).
- Dino, R., Soares, E. A. A., Antonioli, L., Riccomini, C., and Nogueira, A. C. R. (2012). Palynostratigraphy and sedimentary facies of middle miocene fluvial deposits of the amazonas basin, Brazil. *J. S. Am. Earth Sci.* 34, 61–80. doi:10.1016/j.jsames.2011.11.008
- Ermini, L., and Casagli, N. (2003). Prediction of the behaviour of landslide dams using a geomorphological dimensionless index. *Earth Surf. Process. Landforms J. Br. Geomorphol. Res. Group* 28 (1), 31–47. doi:10.1002/esp.424
- Eyles, N., Eyles, C. H., and McCabe, A. M. (1988). Late Pleistocene subaerial debris-flow facies of the bow valley, near banff, Canadian rocky mountains. *Sedimentology* 35 (3), 465–480. doi:10.1111/j.1365-3091.1988.tb00998.x
- Fan, X., Dufresne, A., Subramanian, S. S., Strom, A., Hermanns, R., Stefanelli, C. T., et al. (2020). The formation and impact of landslide dams—State of the art. *Earth-Science Rev.* 203, 103116. doi:10.1016/j.earscirev.2020.103116
- Ferring, C. R. (2020). “Alluvial settings,” in *Encyclopedia of geoarchaeology*. Editors A. S. Gilbert, P. Goldberg, R. D. Mandel, and V. Aldeias (Cham: Springer International Publishing), 1–11.
- Gao, Q., Cui, Z., Tao, Z., Liu, G., and Hong, Y. (2002). The property, age and formation environment of the palaeokarst in Qinghai-Xizang Plateau. *J. Geogr. Sci.* 12 (2), 144–152. doi:10.1007/BF02837468
- Gao, S., and Collins, M. B. (1994). Analysis of grain size trends, for defining sediment transport pathways in marine environments. *J. Coast. Res.* 10 (1), 70–78. doi:10.1002/esp.261
- Gobala krishnan, N., Nagendra, R., and Elango, L. (2015). Quartz surface microtextural studies of Cauvery River sediments, Tamil Nadu, India. *Arabian J. Geosciences* 8 (12), 10665–10673. doi:10.1007/s12517-015-1995-0

- Goudie, A., and Bull, P. A. (1984). Slope process change and colluvium deposition in Swaziland: an SEM analysis. *Earth Surf. Process. Landforms* 9 (3), 289–299. doi:10.1002/esp.3290090308
- Greenbaum, N., Schwartz, U., Carling, P., Bergman, N., Mushkin, A., Zituni, R., et al. (2020). Frequency of boulders transport during large floods in hyperarid areas using paleoflood analysis – an example from the Negev Desert, Israel. *Earth-Science Rev.* 202, 103086. doi:10.1016/j.earscirev.2020.103086
- Guo, Y., Ge, Y., Mao, P., Liu, T., Fu, X., and Wu, S. (2023). Geomorphologic evidences and hydrologic reconstruction of holocene catastrophic flood events in the yarlung tsangpo grand canyon, eastern himalaya. *J. Hydrology* 626, 130146. doi:10.1016/j.jhydrol.2023.130146
- Guo, Y., Huang, C. C., Pang, J., Zhou, Y., Zha, X., and Mao, P. (2017). Reconstruction paleoflood hydrology using slackwater flow depth method in the Yanhe River valley, middle Yellow River basin, China. *J. Hydrology* 544, 156–171. doi:10.1016/j.jhydrol.2016.11.017
- Harms, J. C., Southard, J. B., Spearing, D. R., and Walker, R. G. (1975). *Depositional environments as interpreted from primary sedimentary structures and stratification sequences*. Tulsa, Oklahoma: SEPM Society for Sedimentary Geology.
- Harrison, S., Kargel, J. S., Huggel, C., Reynolds, J., Shugar, D. H., Betts, R. A., et al. (2018). Climate change and the global pattern of moraine-dammed glacial lake outburst floods. *Cryosphere* 12 (4), 1195–1209. doi:10.5194/tc-12-1195-2018
- Herget, J., and Fontana, A. (2019). *Paleohydrology: traces, tracks and trails of extreme events*. Berlin, Heidelberg: Springer.
- Huang, C. C., Pang, J., Zha, X., Zhou, Y., Su, H., and Li, Y. (2010). Extraordinary floods of 4100–4000 a BP recorded at the late neolithic ruins in the jinghe river gorges, middle reach of the yellow river, China. *Palaeogeogr. Palaeoclimatol. Palaeoecol.* 289 (1–4), 1–9. doi:10.1016/j.palaeo.2010.02.003
- Huggel, C., Käab, A., Haeblerli, W., Teysseire, P., and Paul, F. (2002). Remote sensing based assessment of hazards from glacier lake outbursts: a case study in the Swiss Alps. *Can. Geotechnical J.* 39 (2), 316–330. doi:10.1139/t01-099
- Immonen, N. (2013). Surface microtextures of ice-rafted quartz grains revealing glacial ice in the Cenozoic Arctic. *Palaeogeogr. Palaeoclimatol. Palaeoecol.* 374, 293–302. doi:10.1016/j.palaeo.2013.02.003
- Jarrett, R. D., and England, J. F. (2002). “Reliability of paleostage indicators for paleoflood studies,” in *Ancient floods, modern hazards*. Editors P. K. House, R. H. Webb, V. R. Baker, and D. R. Levis, 91–109.
- Jiang, X., Cheng, H., Gao, L., and Liu, W. (2021). The formation and geometry characteristics of boulder bars due to outburst floods triggered by overtopped landslide dam failure. *Earth Surf. Dyn.* 9 (5), 1263–1277. doi:10.5194/esurf-9-1263-2021
- Jiang, X., Huang, J., Wei, Y., Niu, Z., Chen, F., Zou, Z., et al. (2018). The influence of materials on the breaching process of natural dams. *Landslides* 15 (2), 243–255. doi:10.1007/s10346-017-0877-9
- Jiang, X., and Wei, Y. (2019). Natural dam breaching due to overtopping: effects of initial soil moisture. *Bull. Eng. Geol. Environ.* 78 (7), 4821–4831. doi:10.1007/s10064-018-01441-7
- Jiang, X., and Wei, Y. (2020). Erosion characteristics of outburst floods on channel beds under the conditions of different natural dam downstream slope angles. *Landslides* 17 (8), 1823–1834. doi:10.1007/s10346-020-01381-y
- Knox, J. C. (2000). Sensitivity of modern and Holocene floods to climate change. *Quat. Sci. Rev.* 19 (1–5), 439–457. doi:10.1016/S0277-3791(99)00074-8
- Korup, O. (2012). Earth's portfolio of extreme sediment transport events. *Earth-Science Rev.* 112 (3–4), 115–125. doi:10.1016/j.earscirev.2012.02.006
- Korup, O., and Clague, J. J. (2009). Natural hazards, extreme events, and mountain topography. *Quat. Sci. Rev.* 28 (11–12), 977–990. doi:10.1016/j.quascirev.2009.02.021
- Korup, O., and Montgomery, D. R. (2008). Tibetan plateau river incision inhibited by glacial stabilization of the Tsangpo gorge. *Nature* 455 (7214), 786–789. doi:10.1038/nature07322
- Korup, O., Montgomery, D. R., and Hewitt, K. (2010). Glacier and landslide feedbacks to topographic relief in the Himalayan syntaxes. *Proc. Natl. Acad. Sci. U. S. A.* 107 (12), 5317–5322. doi:10.1073/pnas.0907531107
- Li, T., Schuster, R. L., and Wu, J. (1986). “Landslide dams in south-central China,” in *Landslide dams: processes, risk, and mitigation*. Editor R. L. Schuster (Washington: American Society of Civil Engineers).
- Liu, D., Cui, Y., Wang, H., Jin, W., Wu, C., Bazai, N. A., et al. (2021). Assessment of local outburst flood risk from successive landslides: case study of Baige landslide-dammed lake, upper Jinsha river, eastern Tibet. *J. Hydrology* 599, 126294. doi:10.1016/j.jhydrol.2021.126294
- Liu, W., Carling, P. A., Hu, K., Wang, H., Zhou, Z., Zhou, L., et al. (2019). Outburst floods in China: a review. *Earth-Science Rev.* 197, 102895. doi:10.1016/j.earscirev.2019.102895
- Liu, W., Hu, K., Carling, P. A., Lai, Z., Cheng, T., and Xu, Y. (2018). The establishment and influence of Baimakou paleo-dam in an upstream reach of the Yangtze River, southeastern margin of the Tibetan Plateau. *Geomorphology* 321, 167–173. doi:10.1016/j.geomorph.2018.08.028
- Lord, M. L., and Kehew, A. E. (1987). Sedimentology and paleohydrology of glacial-lake outburst deposits in southeastern Saskatchewan and northwestern North Dakota. *Geol. Soc. Am. Bull.* 99 (5), 663–673. doi:10.1130/0016-7606(1987)99<663:SAPOGO>2.0.CO;2
- Ma, J., Chen, J., Cui, Z., Zhou, W., Chen, R., and Wang, C. (2022). Reconstruction of catastrophic outburst floods of the Diexi ancient landslide-dammed lake in the upper Minjiang River, eastern Tibetan plateau. *Nat. Hazards* 112 (2), 1191–1221. doi:10.1007/s11069-022-05223-z
- Ma, J., Chen, J., Cui, Z., Zhou, W., Liu, C., Guo, P., et al. (2018). Sedimentary evidence of outburst deposits induced by the Diexi paleolandslide-dammed lake of the upper Minjiang River in China. *Quat. Int.* 464, 460–481. doi:10.1016/j.quaint.2017.09.022
- Mahaney, W. C., and Kalm, V. (2000). Comparative scanning electron microscopy study of oriented till blocks, glacial grains and Devonian sands in Estonia and Latvia. *Boreas* 29 (1), 35–51. doi:10.1111/j.1502-3885.2000.tb01199.x
- Maizels, J. (1997). Jökulhlaup deposits in proglacial areas. *Quat. Sci. Rev.* 16 (7), 793–819. doi:10.1016/S0277-3791(97)00023-1
- Mao, P., Guo, Y., and Liu, T. (2023). Holocene extreme paleofloods recorded by slackwater deposits along the Jiacha Gorge of the Yarlung Tsangpo River valley, southern Tibetan Plateau. *Catena* 231, 107360. doi:10.1016/j.catena.2023.107360
- Mao, P., Pang, J., Huang, C., Zha, X., Zhou, Y., Guo, Y., et al. (2016). A multi-index analysis of the extraordinary paleoflood events recorded by slackwater deposits in the Yunxi Reach of the upper Hanjiang River, China. *Catena* 145, 1–14. doi:10.1016/j.catena.2016.05.016
- Margolis, S. V., and Krinsley, D. H. (1974). Processes of formation and environmental occurrence of microfossils on detrital quartz grains. *Am. J. Sci.* 274 (5), 449–464. doi:10.2475/ajs.274.5.449
- McKee, E. D., Crosby, E. J., and Berryhill, H. L. (1967). Flood deposits, bijou creek, Colorado, JUNE =). *J. Sediment. Res.* 37 (3), 829–851. doi:10.1306/74D717B2-2B21-11D7-8648000102C1865D
- McManus, J. (1988). “Grain size determination and interpretation,” in *Techniques in sedimentology*. Editor M. E. Tucker (Oxford: Blackwell Scientific Publications), 63–85.
- Miall, A. D. (2013). *The geology of fluvial deposits: sedimentary facies, basin analysis, and petroleum geology*. Berlin, Heidelberg: Springer.
- Miall, A. D. (2022). “Facies models,” in *Stratigraphy: a modern synthesis*. Editor A. D. Miall (Cham: Springer International Publishing), 175–230.
- Molén, M. O. (2014). A simple method to classify diamicts by scanning electron microscope from surface microtextures. *Sedimentology* 61 (7), 2020–2041. doi:10.1111/sed.12127
- Moscariello, A., Marchi, L., Maraga, F., and Mortara, G. (2002). “Alluvial fans in the Italian alps: sedimentary facies and processes,” in *Flood and megaflood processes and deposits*. Editors P. Martini, V. R. Baker, and G. Garzón, 141–166.
- Mutti, E., Tinterri, R., Di Biase, D., Fava, L., Mavilla, N., Angella, S., et al. (2000). Delta-front facies associations of ancient flood-dominated fluvio-deltaic systems. *Rev. Soc. Geol. España* 13 (2), 165–190.
- O'Connor, J. E. (1993). *Hydrology, hydraulics, and geomorphology of the Bonneville flood*. Boulder, CO: Geological Society of America.
- O'Connor, J. E., Clague, J. J., Walder, J. S., Manville, V., and Beebe, R. A. (2022). “6.36 - outburst floods,” in *Treatise on geomorphology*. Editor J. F. Shroder Second Edition (San Diego: Academic Press), 765–819.
- O'Connor, J. E., and Costa, J. E. (2004). *The world's largest floods, past and present: their causes and magnitudes*. Reston, VA: U.S. Geological Survey Circular 1254.
- O'Connor, J. E., Grant, G. E., and Costa, J. E. (2002). “The geology and geography of floods,” in *Ancient floods, modern hazards: principles applications of paleoflood hydrology*. Editors P. K. House, R. H. Webb, and D. R. Levis (Washington: American Geophysical Union), 359–385.
- Peng, M., and Zhang, L. M. (2012). Breaching parameters of landslide dams. *Landslides* 9 (1), 13–31. doi:10.1007/s10346-011-0271-y
- Peng, M., and Zhang, L. M. (2013). Dynamic decision making for dam-break emergency management – Part 2: application to Tangjiashan landslide dam failure. *Nat. Hazards Earth Syst. Sci.* 13 (2), 439–454. doi:10.5194/nhess-13-439-2013
- Quesada-Román, A., Ballesteros-Cánovas, J. A., George, S. S., and Stoffel, M. (2022). Tropical and subtropical dendrochronology: approaches, applications, and prospects. *Ecol. Indic.* 144, 109506. doi:10.1016/j.ecolind.2022.109506
- Ran, Y., Chen, L., Chen, G., Yin, J., Chen, J., Gong, H., et al. (2008). Primary analyses of in-situ recurrence of large earthquake along seismogenic fault of the Ms 8.0 Wenchuan earthquake (in Chinese with English Abstract). *Seismol. Geol.* 30 (3), 630–643. doi:10.3969/j.issn.0253-4967.2008.03.004
- Reading, H. G. (2009). *Sedimentary environments: processes, facies and stratigraphy*. Oxford: Blackwell Publishing.
- RGSTS (1975). *Regional geological survey report of the People's Republic of China: images of Songpan (NO. I-48-XXXII) and Maowen (NO. H-48-II) (scale: 1:200000)*. Chengdu: Regional Geological Survey Team of the Sichuan Bureau of Geology and Mineral Resources.

- Roe, G. H., Baker, M. B., and Herla, F. (2017). Centennial glacier retreat as categorical evidence of regional climate change. *Nat. Geosci.* 10 (2), 95–99. doi:10.1038/ngeo2863
- Ruiz-Bellet, J. L., Castellort, X., Balasch, J. C., and Tuset, J. (2017). Uncertainty of the peak flow reconstruction of the 1907 flood in the ebro River in xerta (NE Iberian peninsula). *J. Hydrology* 545, 339–354. doi:10.1016/j.jhydrol.2016.12.041
- Russell, A. J., and Knudsen, Ó. (1999). An ice-contact rhythmite (turbidite) succession deposited during the November 1996 catastrophic outburst flood (jökulhlaup), Skeiðarárjökull, Iceland. *Sediment. Geol.* 127 (1–2), 1–10. doi:10.1016/S0037-0738(99)00024-X
- Russell, A. J., and Knudsen, Ó. (2002). “The effects of glacier-outburst flood flow dynamics on ice-contact deposits: november 1996 Jökulhlaup, Skeiðarársandur, Iceland,” in *Flood and megaflood processes and deposits*. Editors I. P. Martini, V. R. Baker, and G. Garzón (Chichester: Wiley), 67–83.
- Schmocker, L., Frank, P.-J., and Hager, W. H. (2014). Overtopping dike-breach: effect of grain size distribution. *J. Hydraulic Res.* 52 (4), 559–564. doi:10.1080/00221686.2013.878403
- Shi, Z. M., Guan, S. G., Peng, M., Zhang, L. M., Zhu, Y., and Cai, Q. P. (2015). Cascading breaching of the Tangjiashan landslide dam and two smaller downstream landslide dams. *Eng. Geol.* 193, 445–458. doi:10.1016/j.enggeo.2015.05.021
- Shugar, D. H., Burr, A., Haritashya, U. K., Kargel, J. S., Watson, C. S., Kennedy, M. C., et al. (2020). Rapid worldwide growth of glacial lakes since 1990. *Nat. Clim. Change* 10 (10), 939–945. doi:10.1038/s41558-020-0855-4
- Smith, G. A. (1986). Coarse-grained nonmarine volcanoclastic sediment: terminology and depositional process. *Geol. Soc. Am. Bull.* 97 (1), 1–10. doi:10.1130/0016-7606(1986)97<1:CNVSTA>2.0.CO;2
- Sohn, Y. K., Rhee, C. W., and Kim, B. C. (1999). Debris flow and hyperconcentrated flood-flow deposits in an alluvial fan, northwestern part of the Cretaceous Yongdong Basin, Central Korea. *J. Geol.* 107 (1), 111–132. doi:10.1086/314334
- Srivastava, P., Kumar, A., Chaudhary, S., Meena, N., Sundriyal, Y., Rawat, S., et al. (2017). Paleofloods records in himalaya. *Geomorphology* 284, 17–30. doi:10.1016/j.geomorph.2016.12.011
- Støren, E. W., Paasche, Ø., Hirt, A. M., and Kumari, M. (2016). Magnetic and geochemical signatures of flood layers in a lake system. *Geochem. Geophys. Geosystems* 17 (10), 4236–4253. doi:10.1002/2016GC006540
- Sweet, D. E., and Soreghan, G. S. (2010). Application of Quartz Sand Microtextural Analysis to Infer Cold-Climatic Weathering for the Equatorial Fountain Formation (Pennsylvanian–Permian, Colorado, U.S.A.). *J. Sediment. Res.* 80 (7), 666–677. doi:10.2110/jsr.2010.061
- Taylor, C., Robinson, T. R., Dunning, S., Rachel Carr, J., and Westoby, M. (2023). Glacial lake outburst floods threaten millions globally. *Nat. Commun.* 14, 487. doi:10.1038/s41467-023-36033-x
- Teller, J. T., Leverington, D. W., and Mann, J. D. (2002). Freshwater outbursts to the oceans from glacial Lake Agassiz and their role in climate change during the last deglaciation. *Quat. Sci. Rev.* 21 (8–9), 879–887. doi:10.1016/S0277-3791(01)00145-7
- Tian, S., Chen, N., Wu, H., Yang, C., Zhong, Z., and Rahman, M. (2020). New insights into the occurrence of the Baige landslide along the Jinsha River in Tibet. *Landslides* 17 (5), 1207–1216. doi:10.1007/s10346-020-01351-4
- Van Gorp, W., Schoorl, J. M., Temme, A. J. A. M., Reimann, T., Wijbrans, R., Maddy, D., et al. (2016). Catchment response to lava damming: integrating field observation, geochronology and landscape evolution modelling. *Earth Surf. Process. Landforms* 41 (11), 1629–1644. doi:10.1002/esp.3981
- Visher, G. S. (1969). Grain size distributions and depositional processes. *J. Sediment. Res.* 39 (3), 1074–1106. doi:10.1306/74D71D9D-2B21-11D7-8648000102C1865D
- Vos, K., Vandenbergh, N., and Elsen, J. (2014). Surface textural analysis of quartz grains by scanning electron microscopy (SEM): From sample preparation to environmental interpretation. *Earth-Science Rev.* 128, 93–104. doi:10.1016/j.earscirev.2013.10.013
- Walder, J. S., Iverson, R. M., Godt, J. W., Logan, M., and Solovitz, S. A. (2015). Controls on the breach geometry and flood hydrograph during overtopping of noncohesive earthen dams. *Water Resour. Res.* 51 (8), 6701–6724. doi:10.1002/2014WR016620
- Wang, H., Cui, P., Yang, A., Tang, J., Wen, S., Yang, Z., et al. (2023a). New evidence of high-magnitude Holocene floods in the Purlung Tsangpo River, southeastern Tibetan Plateau. *Catena* 233, 107516. doi:10.1016/j.catena.2023.107516
- Wang, H., Cui, P., Zhou, L., Liu, W., Yang, A., Yao, S., et al. (2022a). Spatial and temporal distribution of landslide-dammed lakes in Purlung Tsangpo. *Eng. Geol.* 308, 106802. doi:10.1016/j.enggeo.2022.106802
- Wang, H., Yang, A., Jiang, S., and Liu, N. (2023b). Reconstruction of a Holocene landslide-dammed lake in the Yalong basin, eastern Tibetan Plateau. *Front. Earth Sci.* 10, 1042581. doi:10.3389/feart.2022.1042581
- Wang, L., Huang, C. C., Pang, J., Zha, X., and Zhou, Y. (2014a). Paleofloods recorded by slackwater deposits in the upper reaches of the Hanjiang River valley, middle Yangtze River basin, China. *J. Hydrology* 519, 1249–1256. doi:10.1016/j.jhydrol.2014.08.002
- Wang, P., Chen, J., Dai, F., Long, W., Xu, C., Sun, J., et al. (2014b). Chronology of relict lake deposits around the Suwalong paleolandslide in the upper Jinsha River, SE Tibetan Plateau: Implications to Holocene tectonic perturbations. *Geomorphology* 217, 193–203. doi:10.1016/j.geomorph.2014.04.027
- Wang, P., Zhang, B., Qiu, W., and Wang, J. (2011). Soft-sediment deformation structures from the Diexi paleo-dammed lakes in the upper reaches of the Minjiang River, east Tibet. *J. Asian Earth Sci.* 40 (4), 865–872. doi:10.1016/j.jseas.2010.04.006
- Wang, Z., Yue, G., Lin, H., and Li, M. (2022b). Numerical analysis of dynamic evolution characteristics of a large rock landslide in Tangjiashan. *Geofluids* 2022, 1–17. doi:10.1155/2022/5423743
- Wohl, E. E. (1992). Bedrock benches and boulder bars: Floods in the Burdekin Gorge of Australia. *Geol. Soc. Am. Bull.* 104 (6), 770–778. doi:10.1130/0016-7606(1992)104<0770:BBABBF>2.3.CO;2
- Wu, H., Trigg, M. A., Murphy, W., and Fuentes, R. (2022). A new global landslide dam database (RAGLAD) and analysis utilizing auxiliary global fluvial datasets. *Landslides* 19 (3), 555–572. doi:10.1007/s10346-021-01817-z
- Xiong, X., Matsumoto, T., Shi, Z., and Zhang, F. (2022). Flume tests and corresponding numerical simulation of hydraulic/mechanical behavior of Tangjiashan landslide dam subjected to seepage loading. *Soils Found.* 62 (5), 101200. doi:10.1016/j.sandf.2022.101200
- Xue, B., Wang, S., Xia, W., Wu, J., Wang, Y., Qian, J., et al. (1998). The uplifting and environmental change of Qinghai-Xizang (Tibetan) Plateau in the past 0.9 Ma inferred from core RM of Zoige Basin. *Sci. China Ser. D Earth Sci.* 41 (2), 165–170. doi:10.1007/BF02932436
- Yang, A., Wang, H., Liu, W., Hu, K., Liu, D., Wu, C., et al. (2022). Two megafloods in the middle reach of Yarlung Tsangpo River since Last-glacial period: Evidence from giant bars. *Glob. Planet. Change* 208, 103726. doi:10.1016/j.gloplacha.2021.103726
- Zhang, P. (2013). A review on active tectonics and deep crustal processes of the Western Sichuan region, eastern margin of the Tibetan Plateau. *Tectonophysics* 584, 7–22. doi:10.1016/j.tecto.2012.02.021
- Zhang, Q., Chen, Z., Li, Y., Yu, S., Wang, L., Zhou, X., et al. (2023). Quantitative assessment on landslide dam risks and mitigation: an in-depth study on the Baige lake breach. *Environ. Earth Sci.* 82 (4), 96–20. doi:10.1007/s12665-023-10778-6
- Zhao, T., Crosta, G. B., Dai, F., and Xu, N. (2018). “Generation of complex slope geometries by DEM for modeling landslides: A case study of Tangjiashan landslide,” in *GeoShanghai 2018 international conference: geoenvironment and geohazard*. Editors A. Farid, and H. Chen (Singapore: Springer).
- Zheng, H., Shi, Z., Shen, D., Peng, M., Hanley, K. J., Ma, C., et al. (2021). Recent advances in stability and failure mechanisms of landslide dams. *Front. Earth Sci.* 9, 659935. doi:10.3389/feart.2021.659935
- Zhong, Q., Chen, S., Wang, L., and Shan, Y. (2020). Back analysis of breaching process of Baige landslide dam. *Landslides* 17 (7), 1681–1692. doi:10.1007/s10346-020-01398-3
- Zhong, Q., Wang, L., Chen, S., Chen, Z., Shan, Y., Zhang, Q., et al. (2021). Breaches of embankment and landslide dams - State of the art review. *Earth-Science Rev.* 216, 103597. doi:10.1016/j.earscirev.2021.103597
- Zhou, G. G. D., Zhou, M., Shrestha, M. S., Song, D., Choi, C. E., Cui, K. F. E., et al. (2019). Experimental investigation on the longitudinal evolution of landslide dam breaching and outburst floods. *Geomorphology* 334, 29–43. doi:10.1016/j.geomorph.2019.02.035
- Zhu, X., Peng, J., Jiang, C., and Guo, W. (2019). A Preliminary study of the failure modes and process of landslide dams due to upstream flow. *Water* 11 (6), 1115. doi:10.3390/w11061115